This article was downloaded by:
On: *21 January 2011*
Access details: *Access Details: Free Access*
Publisher *Taylor & Francis*
Informa Ltd Registered in England and Wales Registered Number: 1072954 Registered office: Mortimer House, 37-41 Mortimer Street, London W1T 3JH, UK

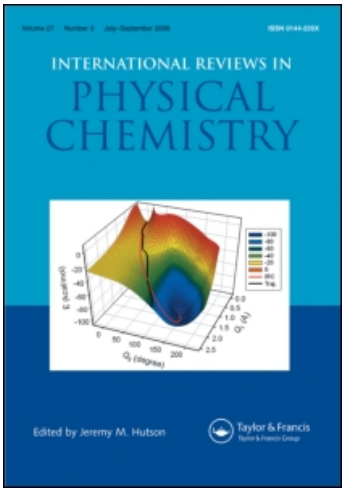

International Reviews in Physical Chemistry
Publication details, including instructions for authors and subscription information:
http://www.informaworld.com/smpp/title~content=t713724383

Photoionisation and photodissociation studies of nonvolatile organic molecules by synchrotron VUV photoionisation mass spectrometry and theoretical calculations

Yang Pan[a]; Lidong Zhang[a]; Huijun Guo[a]; Liulin Deng[a]; Fei Qi[a]
[a] National Synchrotron Radiation Laboratory, University of Science and Technology of China, Hefei, P. R. China

Online publication date: 15 April 2010

To cite this Article Pan, Yang , Zhang, Lidong , Guo, Huijun , Deng, Liulin and Qi, Fei(2010) 'Photoionisation and photodissociation studies of nonvolatile organic molecules by synchrotron VUV photoionisation mass spectrometry and theoretical calculations', International Reviews in Physical Chemistry, 29: 2, 369 — 401
To link to this Article: DOI: 10.1080/01442351003668697
URL: http://dx.doi.org/10.1080/01442351003668697

PLEASE SCROLL DOWN FOR ARTICLE

Full terms and conditions of use: http://www.informaworld.com/terms-and-conditions-of-access.pdf

This article may be used for research, teaching and private study purposes. Any substantial or systematic reproduction, re-distribution, re-selling, loan or sub-licensing, systematic supply or distribution in any form to anyone is expressly forbidden.

The publisher does not give any warranty express or implied or make any representation that the contents will be complete or accurate or up to date. The accuracy of any instructions, formulae and drug doses should be independently verified with primary sources. The publisher shall not be liable for any loss, actions, claims, proceedings, demand or costs or damages whatsoever or howsoever caused arising directly or indirectly in connection with or arising out of the use of this material.

International Reviews in Physical Chemistry
Vol. 29, No. 2, April–June 2010, 369–401

Taylor & Francis
Taylor & Francis Group

Photoionisation and photodissociation studies of nonvolatile organic molecules by synchrotron VUV photoionisation mass spectrometry and theoretical calculations

Yang Pan, Lidong Zhang, Huijun Guo, Liulin Deng and Fei Qi*

National Synchrotron Radiation Laboratory, University of Science and Technology of China, Anhui 230029, Hefei, P. R. China

(*Received 30 November 2009; final version received 21 January 2010*)

The importance of photo-induced ionisation and dissociation of organic molecules has been recognised for several decades. Many studies have been carried out with different techniques and methods. However, introducing nonvolatile and thermally labile compounds into the gas phase in an ionisation chamber under high vacuum is still a great challenge. In this review, we present our recent work on the photoionisation and photodissociation of a series of nonvolatile organic molecules using IR laser desorption combined with tunable synchrotron vacuum ultraviolet photoionisation mass spectrometry. The fundamental fragmentation pathways of these compounds are discussed in detail. Theoretical calculations are employed in order to compare theoretical and experimental outcomes. We also give the potential application of this method in the qualitative analysis of complex mixtures.

Keywords: nonvolatile organic molecules; infrared laser desorption; photoionisation mass spectrometry; synchrotron; vacuum ultraviolet; theoretical calculations

Downloaded At: 15:33 21 January 2011

Contents

*Corresponding author. Email: fqi@ustc.edu.cn

ISSN 0144–235X print/ISSN 1366–591X online
© 2010 Taylor & Francis
DOI: 10.1080/01442351003668697
http://www.informaworld.com

Downloaded At: 15:33 21 January 2011

1. Introduction

1.1. *Synchrotron vacuum ultraviolet photoionisation mass spectrometry*

The interaction of electromagnetic fields with different types of matter has been investigated for over 100 years; the photoelectric effect was first observed by Hertz in 1887 and explained by Einstein in 1905 [1–4]. The studies of this phenomenon in the gas phase allow the examination of photoionisation processes in free atoms and molecules, which are of great importance for numerous physical systems, including a large variety of astrophysical systems, the upper atmosphere, different types of laboratory plasma, etc. [5]. Since the first paper on the photoionisation of atoms and molecules, much work has been reported in various fields [3].

The first measurement of photoionisation was carried out by Mohler and Boeckner in 1926 [6] on alkali metal vapours using light in the near-ultraviolet region. The additional techniques for investigations in the vacuum ultraviolet (VUV) region were developed after World War II [7], by which absorption cross sections, photoionisation efficiency (PIE) and ionisation energies (IEs) could be measured properly [8–11]. Photoionisation was first combined with mass spectrometry by Lossing and Tanaka [12] in 1956. Mass spectrometric measurements remove all uncertainties regarding the identity of the ionisation process and prevent interference from impurities. One year later, this technique was improved by using a VUV monochromator. By virtue of this innovation, the PIE spectra of molecular and fragment ions from a number of molecules can be measured, from which

IEs and appearance energies (AEs) of fragments can be obtained [13]. As IEs and AEs are related to 0 K bond dissociation energies of neutrals and cations, such values are of fundamental importance to chemistry [14]. Traditionally, photoionisation measurements are implemented with discharge lamps filled with different gases. The significant advances in photoionisation mass spectrometry are attributed to the innovative development of modern light sources, such as VUV lasers and synchrotron radiation facilities, etc. [14]. With high tunability and energy resolution in the VUV range, the synchrotron photoionisation mass spectrometry has become a prominent technique in many research fields [15–18].

Generally, synchrotron-based photoionisation processes take place in a high-vacuum chamber (approximately 10^{-4} Pa), in which the samples introduced are limited to gaseous and volatile condensed matter. As for nonvolatile samples, evaporation by heating is conventionally used, as adopted by Jochims and coworkers [18–20] in the studies on a series of amino acids and DNA bases at BESSY. Our group has also used this heating method to study the photodissociation and pyrolysis of polymers by synchrotron photoionisation mass spectrometry [21]. However, this method is only suitable for a small number of thermally stable molecules, which do not decompose at a relatively high temperature. Ahmed and coworkers [22,23] used an aerosol particle mass spectrometer (APMS) coupled to VUV synchrotron facility at the advanced light source (ALS) to study some amino acids, where nanoparticles of analytes were impacted onto a heater button. We have also used electrospray in combination with photoionisation mass spectrometry to investigate some solid samples, where fine droplets of the sample solution were electrosprayed into a high-vacuum chamber and were subsequently ionised by tunable synchrotron VUV light [24].

Downloaded At: 15:33 21 January 2011

1.2. *Laser desorption-based mass spectrometry*

The emergence of laser techniques has opened numerous opportunities for its applications in many fields. The laser desorption/ionisation mass spectrometry (LDI MS) is a combination of laser and mass spectrometer, which has been studied during the past several decades [1,25–28]. Time-of-flight (TOF) mass spectrometers were usually employed as the mass analyser. Generally, this method has two major applications: (1) the elemental analysis of solids by ionisation of surface and (2) the structural identification of organic molecules [27]. Earlier, the LDI MS suffered from some deficiencies such as lack of speed and sensitivity [27], which were overcome by the subsequent technological developments, especially the availability of commercial laser microprobe mass spectrometer [29,30].

The LDI MS always produces many fragments. In addition, it was found that at a power density of approximately 10^6 W/cm^2, the number of desorbed neutral molecules would exceed the number of desorbed molecular ions [31]. Thus, a two-step laser mass spectrometry (L2MS) was developed from the LDI, where desorption and ionisation processes are separated temporally and spatially. The L2MS uses laser for desorption followed by the resonance-enhanced multiphoton ionisation (REMPI) with laser or single-photon ionisation (SPI) with laser/discharge lamp to produce ions [32]. Due to the 'soft' ionisation, especially for SPI, the L2MS requires almost no sample preparation [33] and has proven to be a powerful analytical technique for characterising a wide range of molecular systems with high sensitivity [34–46].

Another well-known technique is the matrix-assisted laser desorption/ionisation (MALDI) mass spectrometry, which was introduced by Tanaka *et al.* [47] in 1988. This technique utilises a beam of 337 nm laser to desorb and ionise the sample dissolved in an organic matrix, and has become a standard technique for the analysis of biological macromolecules [48].

1.3. *IR laser desorption/tunable VUV photoionisation mass spectrometry*

Based on the previous pioneering works, we recently constructed an apparatus combining the IR laser desorption with tunable synchrotron VUV photoionisation mass spectrometry (IR LD/VUV PIMS) for the study of photoionisation and photodissociation of nonvolatile organic compounds [49]. In this approach, a beam of IR laser (1064 nm) is used to desorb the analyte deposited on a stainless steel target. Hall [50] has pointed out that metal surfaces can be heated by pulsed lasers at an extremely high rate (over 10^{11} K/s). Owing to the rapid heating effect, neutral samples are quickly evaporated before they have time to kinetically decompose [51]. The samples are then ionised by a crossed VUV light, resembling the operation manner of L2MS. The IR LD/VUV PIMS has been successfully applied for the studies of a variety of small compounds, including polycyclic aromatic hydrocarbons (PAHs), amino acids [52,53], steroids [54], drugs [55], quinones [56,57], DNA bases and complex mixtures [58].

Downloaded At: 15:33 21 January 2011

In our experiments, the laser power is controlled at a relatively low level in order to eliminate the IR multiphoton ionisation and dissociation processes. We show that the production of the mass signal requires contributions from both the IR laser desorption and synchrotron VUV ionisation. No ions could be detected with only the operation of IR laser or synchrotron VUV light [49]. For an isolated molecule, with photon energy slightly higher than the IE of the analyte, only pure molecular ions are produced by virtue of near-threshold photoionisation, with nearly no fragments, as shown in Figure 1. The characteristic fragments of analytes can be seen by gradually increasing the photon energies. Figure 2 demonstrates the photoionisation and photodissociation processes of uridine, a fragile nucleoside, with the variation of photon energies [49]. Compared with the results from IR LD/VUV PIMS, very strong fragmentation was observed for uridine with the electron impact ionisation mass spectrometry (EI-MS) even at low electron energy, and nearly no molecular ion signal was observed [59].

The IR LD/VUV PIMS exhibits several advantages: first, it is a matrix-free mass spectrometric method for organic compound analysis, particularly convenient for nonvolatile and thermally labile molecules. Second, the fragment-free mass spectra can be obtained via near-threshold photoionisation [60]. Under such circumstances, organic mixtures can be identified *in situ* at optimal ionisation photon energy with minimum fragmentation. Third, the isomers with different IEs can be distinguished by measuring their PIE spectrum [61,62]. Fourth, the photo-induced ionisation/dissociation behaviours of analytes can be observed on the mass spectra at different photon energies. Accordingly, the structural information and fragmental evolution processes of an unknown analyte can be deduced.

In the rest of this review, we will begin by introducing the experimental setup of the IR LD/VUV PIMS and the theoretical methods employed. Next, the PIE spectral measurements for neutrals and fragments and existing problems are discussed.

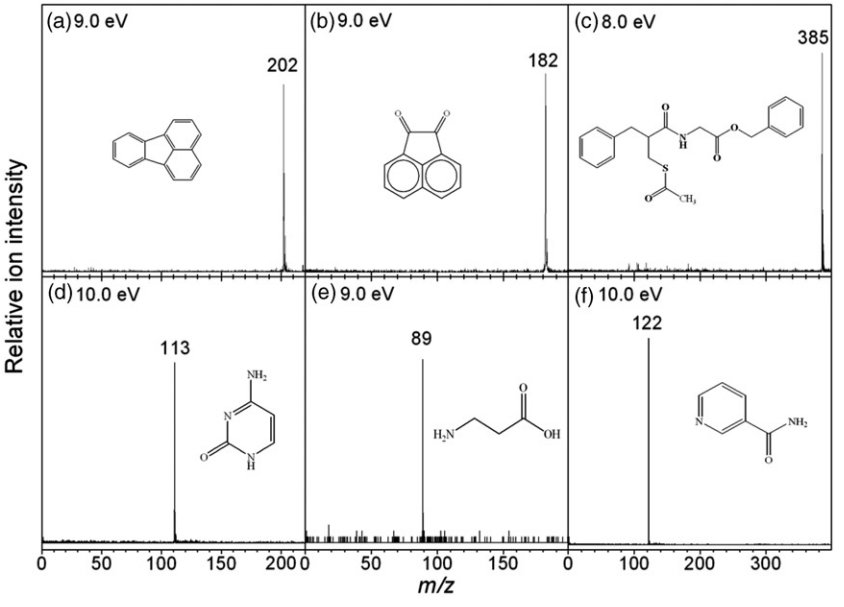

Figure 1. Photoionisation mass spectra of six typical compounds obtained with different VUV photon energies labelled on the figures [49]: (a) mass spectrum of fluoranthene (laser energy = 0.1 mJ/pulse); (b) mass spectrum of 1,2-acenaphthylenedione (laser energy = 1.0 mJ/pulse); (c) mass spectrum of racecadotril (laser energy = 8.5 mJ/pulse); (d) mass spectrum of cytosine (laser energy = 9.6 mJ/pulse); (e) mass spectrum of β-alanine (laser energy = 10.8 mJ/pulse) and (f) mass spectrum of nicotinamide (laser energy = 7.5 mJ/pulse).

Downloaded At: 15:33 21 January 2011

Recent results for the photoionisation and photodissociation processes as well as the fragmentation pathways of several kinds of compounds are then discussed with the help of theoretical calculations. Finally, we will conclude the review, pointing out what questions remain, and talk about our future plans.

2. Experimental apparatus and theoretical method

2.1. *Experimental apparatus*

The instrument of IR LD/VUV PIMS has been reported elsewhere [49,55,57]. Therefore, only a short description is given here. All the samples in our work were commercially obtained and used without further purification. The sample was coated on a stainless steel substrate without any organic matrix. IR LD/VUV PIMS utilised 1064 nm output of a pulsed Nd:YAG laser (Surelite I-20, Continuum, USA) at the operation rate of 10 Hz for the laser desorption on the substrate. The laser beam was focussed to a spot of 0.5–1.0 mm in diameter on the surface of the substrate. The laser power was controlled at about 0.1–10 mJ/pulse to generate intact neutral molecules for near-threshold VUV photoionisation. The tunable VUV light beam from a synchrotron was perpendicular and overlapping with the desorption plume in the photoionisation region. The VUV photoionisation took place at a distance of 1–4 mm from the substrate surface, where

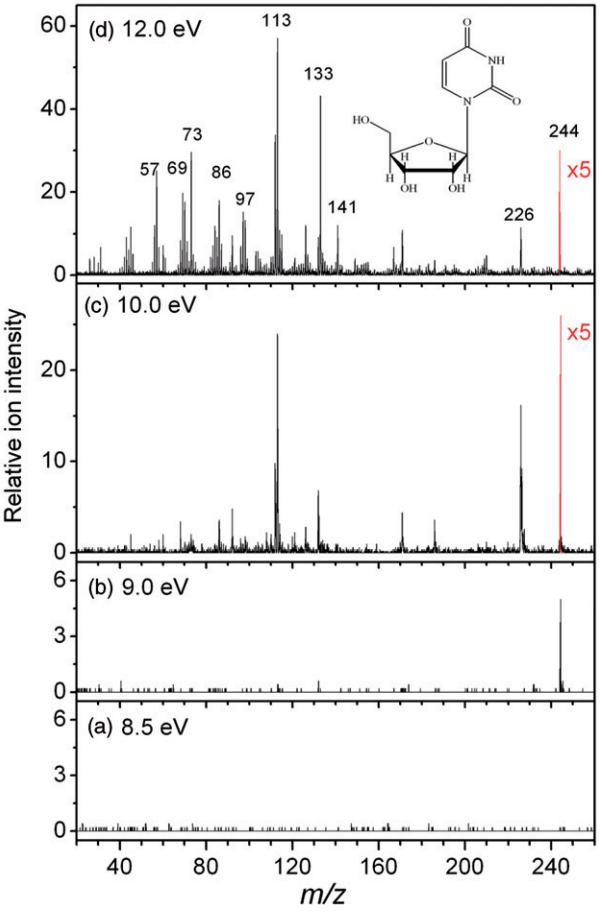

Figure 2. [Colour online]. Photoionisation mass spectra of uridine with different VUV photon energies labelled on the figure (laser energy = 11.0 mJ/pulse) [49]. A large number of fragments are formed at high photon energy. The peak at m/z 244 is amplified fivefold at the photon energy of 10.0 eV (and 12.0 eV), as labelled in the figure.

the plume of molecules formed from the desorption travelled back and was ionised by the VUV light, as shown schematically in Figure 3(a). The ions produced by the VUV light were analysed by a home-made reflectron TOF mass spectrometer [63,64]. A pulsed voltage of 260 V with the frequency of 10 kHz applied to the repeller plates was used to extract ions into the flight tube. The acceleration voltage was kept at 2000 V. The time delay between the Nd:YAG laser and the pulse of the extract field was 150 μs, which was controlled by a home-made pulse/delay generator. The time series between the Nd:YAG laser and the extractor field and multiscaler start is shown in Figure 3(b) [57]. The ion signals were detected with microchannel plates (MCP), and then amplified by a preamplifier (VT120C, ORTEC, USA). A multiscaler (FAST Comtec P7888, Germany) recorded the TOF spectrum with the bin width of 2 ns. A small bias voltage (1.0 V) was used to improve signal intensity, reduce the background ions and enhance the

Downloaded At: 15:33 21 January 2011

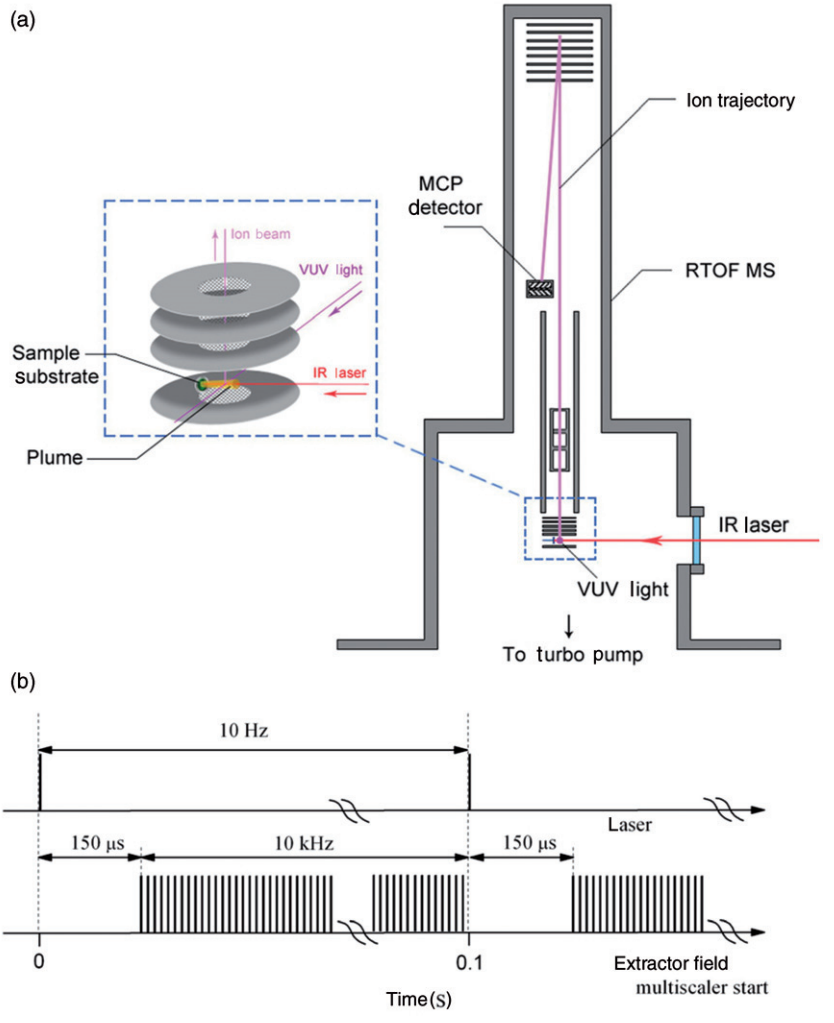

Figure 3. [Colour online]. (a) Schematic setup of an IR laser desorption/VUV photoionisation mass spectrometry – the substrate was placed between the repeller and extractor plates [57]; and (b) time series between the Nd: YAG laser and the extractor field and multiscaler start [57].

mass resolution [63]. The pressure of the photoionisation chamber was approximately 1.0×10^{-4} Pa.

The synchrotron radiation from an undulator of the 800 MeV electron storage ring of National Synchrotron Radiation Laboratory (NSRL) was monochromatised with a 1 m Seya-Namioka monochromator equipped with a laminar grating (1500 grooves/mm, Horiba Jobin Yvon, France). This grating covered the photon energy from 7.8 to 24.0 eV. The monochromator was calibrated with the known IEs of the inert gases. The energy resolving power ($E/\Delta E$) was about 1000. A gas filter filled with neon or argon was used to eliminate higher order radiation. The average photon flux was measured to be around

Downloaded At: 15:33 21 January 2011

1×10^{13} photons/s. A silicon photodiode (SXUV-100, International Radiation Detectors, Inc., USA) was used to monitor the photon flux for normalising ion signals.

2.2. *Theoretical method*

To obtain our theoretical results, the G3B3 and density functional theory (DFT) calculations were carried out with the Gaussian 03 program package [65–68]. The high-level G3B3 method involves single-point calculations at the levels of QCISD(T,E4T)/6-31G(d), MP4/6-31+G(d), MP4/6-31G(2df,p) and MP2(Full)/G3large, based on the structures optimised at the B3LYP/6-31G(d) level. The B3LYP/6-31G(d) harmonic vibrational frequencies, scaled by 0.96, were used for the correction of the zero-point vibrational energies (ZPVE). A semi-empirical correction was also applied to account for the high level correlation (ELC) effect: $E(HLC) = -An_\beta - B(n_\alpha - n_\beta)$, where n_α and n_β are the numbers of α and β valence electrons with $n_\alpha \geq n_\beta$; $A = 10.041$ mhartrees, $B = 4.995$ mhartrees for molecules; $A = 10.188$ mhartrees, $B = 2.323$ mhartrees for atoms. A large number of molecules have been calculated using this method, and good correlation between the G3B3 results and the experimental data has been found [69,70].

Downloaded At: 15:33 21 January 2011

3. PIE spectral measurements

3.1. *PIE spectral measurements of neutral molecules*

Due to the high tunability of synchrotron radiation, the accurate thermodynamic data, such as IEs and AEs, can be obtained by measuring the PIE spectra, which are achieved by plotting the integrated mass peak versus the corresponding photon energy. In our experiments, a laser was used directly to desorb the sample deposited on a target, inevitably making the analyte rotationally and vibrationally hot. Thus, the PIE spectrum will exhibit gradual onsets and extend towards lower photon energies. Such an ambiguous feature makes it difficult to extract accurate IEs from the spectrum. If the signal intensity is high enough, the first departure from background (observable onset) is always somewhat smaller than the 0 K adiabatic IE value. On the other hand, the first onset is related to the strength of the observable ion, which is affected by several factors, such as the intensity of light source, ionisation cross section, counting time and other probable reasons. Therefore, sometimes the experimental IE will be higher than the true IE, if the ion intensity is not detectable at the threshold energy.

We have used the IR LD/VUV PIMS to measure the PIE spectra of several types of compounds, including quinones, amino acids, DNA bases and nucleosides. Figures 4 and 5 show the PIE spectra of 9,10-phenanthroquinone (9,10-PQ), β-alanine and their major fragments [53,57]. The approximate IE values were estimated to be 8.6 and 8.9 ± 0.1 eV for 9,10-PQ and β-alanine, respectively, based on the first discernable onsets. Due to the lack of knowledge about actual temperature and internal energy of desorbates, such a result is simply an approximation. We should emphasise that these experimental values are only estimated adiabatic IEs, as the underlying physics of the photoionisation processes has not been taken into account. The measured IEs for several species studied as part of this review are listed in Table 1. We note that the measured IEs of quinones are similar to those reported previously. For example, our measured IEs for 1,4-naphthoquinone (1,4-NQ) and 9,10-anthraquinone (9,10-AQ) are 9.5 and 9.2 ± 0.1 eV,

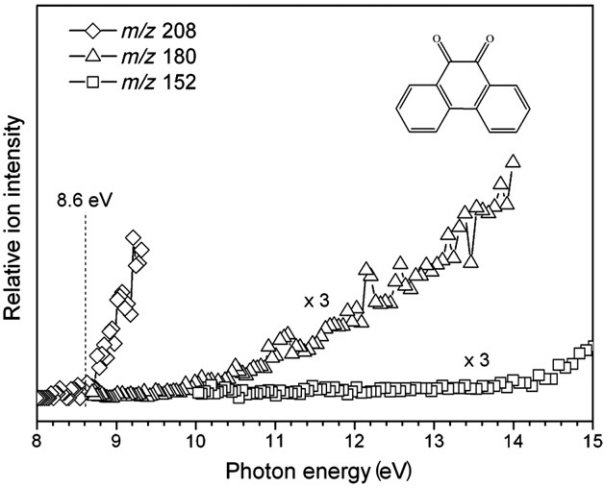

Figure 4. PIE spectra of 9,10-PQ (m/z 208) and its major fragments at m/z 180 and 152. The curves of m/z 180 and 152 are amplified threefold.

Downloaded At: 15:33 21 January 2011

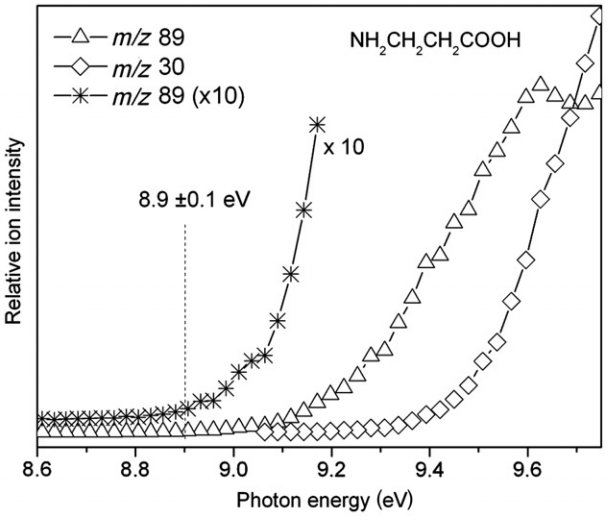

Figure 5. PIE spectra of β-alanine (m/z 89) and its major fragment at m/z 30. Part of the curve of m/z 89 is amplified tenfold [53].

respectively, which are in good agreement with the values (9.5 ± 0.1 and 9.25 ± 0.12 eV, respectively) from NIST [71]. Such a good agreement could be due to the low power density of IR laser impinging on the analytes. Similar to PAHs, these quinones will produce high signal intensities with just a very low incident laser power. The IEs of α-alanine, β-alanine and thymine are determined to be 8.8, 8.8 and 8.9 ± 0.1 eV, respectively, which are also close to the reported data in the literature. The measured IE

Table 1. IEs of some selected compounds.

Compound	*m*/*z*	IE (eV)	
		This work	Literature data
1,4-Naphthoquinone	158	9.5 ± 0.1 [57]	9.5 ± 0.1 [71]
9,10-Anthraquinone	208	9.2 ± 0.1 [57]	9.25 ± 0.12 [71]
9,10-Phenanthroquinone	208	8.6 ± 0.1 [57]	8.64 ± 0.03 [71]
1,2-Acenaphthylenedione	182	8.6 ± 0.1 [57]	8.77 ± 0.05 (vertical) [71]
α-Alanine	89	8.8 ± 0.1 [52]	8.75 ± 0.05 [20]
β-Alanine	89	8.9 ± 0.1 [53]	8.8 ± 0.1 [20]
Thymine	126	8.9 ± 0.1 [unpublished]	8.82 ± 0.03 [18]
Uridine	244	8.7 ± 0.1 [unpublished]	9.05 ± 0.15 (EI) [59]

Note: References are given within square brackets.

of uridine is 8.7 ± 0.1 eV, which is lower than the experimental IE of 9.05 ± 0.15 eV obtained from an EI process [59].

Downloaded At: 15:33 21 January 2011

3.2. *PIE spectral measurements of fragments*

On the other hand, the accurate measurements of AEs of fragment ions are difficult to achieve. The internal rotational and vibrational energy-induced thermal tail asymptotically approaches the baseline. In addition, the kinetic shift will also make the onset hard to be detected. As shown in Figure 4, although the PIE spectra of fragments at *m*/*z* 180 and 152 are amplified threefold, the onsets are still difficult to determine. Guyon and Berkowitz [72] have pointed out the fact that the thermal tail becomes indistinguishable from the background has nothing to do with the AE. Thus, an attempt to report any discernable onset cannot be reasonably justified at this point, due to lack of a logical correction.

4. Photoionisation and photodissociation studies on drugs

Innovations in technique of mass spectrometer make it an unparalleled tool for drug discovery, structural analysis and fragmentation study [73–75]. Currently, the gas chromatography/electron impact ionization mass spectrometry (GC/EI-MS) is universally used and is an easily performed methodology for a wide range of drugs [76]. However, evaporisation before ionisation and high impact energy always result in the loss of molecular ion. The liquid chromatography/electrospray mass spectrometry (LC/ESI-MS) or LC/ESI-MS-MS has also been a common strategy for the analysis of drugs and their possible metabolites since the introduction of ESI by Yamashita and Fenn [77] in the 1980s. Nevertheless, the ESI is not sensitive to nonpolar molecules and is vulnerable to ionisation suppression from biological matrices resulting in inconsistent analytical outcomes [76,78,79]. We have compared the performances of IR LD/VUV PIMS with EI-MS on the ionisation of three different types of drugs, i.e. captopril, fudosteine and

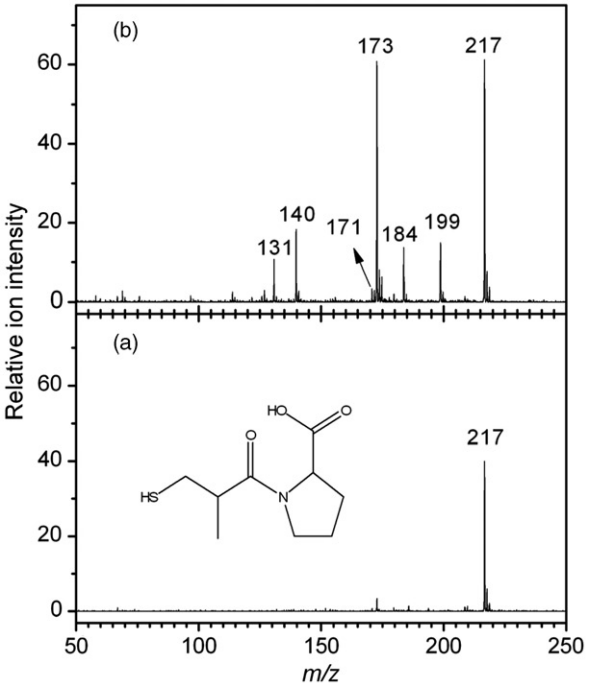

Figure 6. Photoionisation mass spectra of captopril at the photon energies of (a) 9.0 and (b) 10.5 eV [55].

Downloaded At: 15:33 21 January 2011

racecadotril, and demonstrated that IR LD/VUV PIMS gives higher efficiency in ionising and dissociating these drugs even at low excitation photon energy [55].

4.1. *Captopril*

Captopril is generally used for the treatment of hypertension, heart failure and left ventricular dysfunction after myocardial infarction [80]. It consists of a five-membered heterocyclic ring and a carbon chain ending with an unstable mercapto group (SH) which tends to be oxidised in peripheral tissues. Hence, the derivatisation of captopril is necessary before the ESI analysis [81]. Relatively low photon energy of 9.0 eV could yield the molecular ion (M^+) signal at m/z 217 accompanied with minor fragments. More fragments will be formed by increasing the photon energy to 10.5 eV, as shown in Figure 6. The signal at m/z 173 is the base peak, which is due to the loss of neutral CO_2 after C–C bond fission [78]. In addition, other fragments at m/z 199, 184, 140, 131 with relative high intensities are also formed at 10.5 eV. The fragment at m/z 199 is assigned to the loss of water after an intramolecular hydrogen transfer process. The subsequent ejection of neutral carbon monoxide from the ion of m/z 199 will produce the fragment at m/z 171 with relatively low intensity. The mercapto radical loss from the molecular ion results in the fragment ion at m/z 184. After that, the intramolecular hydrogen transfer and subsequent decarboxylation processes occur to yield the m/z 140 ion. The consecutive

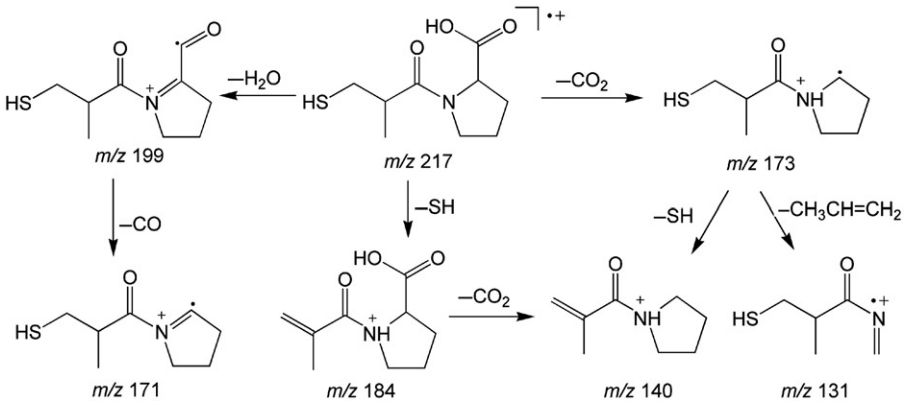

Scheme 1. Proposed fragmentation pathways for the captopril cation [55].

loss of carbon dioxide and mercapto radical from captopril radical cation will also form the fragment at m/z 140. Product ion at m/z 131 may be a fragment ion from m/z 173 by cyclic cleavage with concomitant neutral loss of propene. A schematic representation of the major fragmentation pathways is displayed in Scheme 1. Further increase in the excitation energy will enrich the mass spectrum and vary the relative abundances of the ions. For example, in the mass spectrum from 70 eV EI experiment, the base peak is replaced by the ion at m/z 70, and the relative abundance of the m/z 173 ion is only 6.8% [71].

Downloaded At: 15:33 21 January 2011

4.2. *Fudosteine*

Fudosteine is a derivative of cysteine with a very fragile structure. A small amount of excess energy above the IE will lead to the formation of the fragment ion m/z 75 (Figure 7), similar to the behaviour of cysteine undergoing EI and collision-induced dissociation (CID) processes [71,82]. This dominant fragment is produced from the loss of a neutral carbene $HO(CH_2)_3SCH$ via C–C bond fission after intramolecular hydrogen transfer from carbon atom to nitrogen atom. Due to the resonance effect, the m/z 75 ion is highly stable. At the photon energy of 9.5 eV, complex fragments at m/z 162, 137, 105, 92, 91, 87, 57, and so on are also formed with various yields, as shown in Figure 7. The m/z 162 ion is formed by the loss of a neutral ammonia from the molecular ion M^+ after intramolecular hydrogen transfer, as observed from the CID behaviour of *bis*-methylated carbocysteine, a derivative of fudosteine [83]. The fragment at m/z 134 should originate from the loss of hydrocarboxyl radical from the molecular ion. The product ion at m/z 105 is reasonably assigned to the loss of $CHNH_2COOH$ radical from M^+. A loss of water from this product ion yields the m/z 87 ion. Simple S–C bond fission is responsible for the production of the m/z 92 ion. The β-alanine cation (m/z 89) can also be detected from this bond cleavage pathway [84]. A second formation pathway of m/z 92 can be initiated by the consecutive losses of neutral ammonia and propiolic acid (CHCCOOH) from M^+. The product ion at m/z 58 is assigned to the 2-propenol ion which results from the loss of hydrogen sulfide from m/z 92 ion. All these proposed dissociation pathways are summarised in Scheme 2.

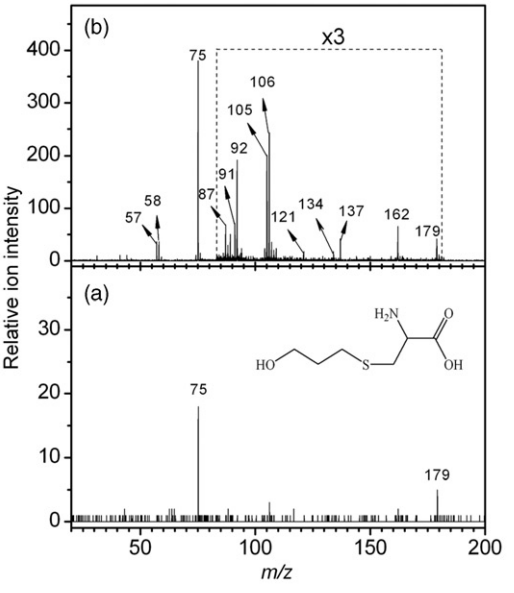

Figure 7. Photoionisation mass spectra of fudosteine at the photon energies of (a) 8.5 and (b) 9.5 eV. Part of the spectrum is amplified by a factor of 3, as labelled in the figure [55].

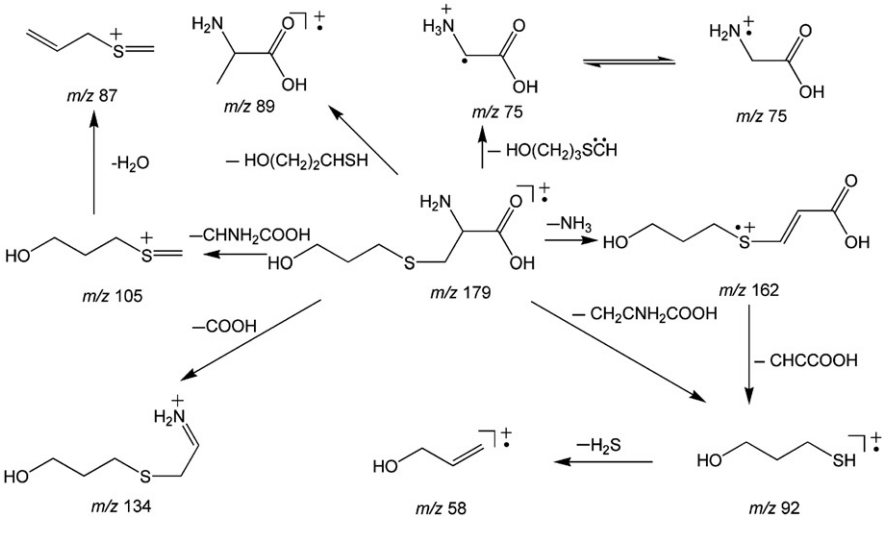

Scheme 2. Proposed fragmentation pathways for the fudosteine cation [55].

4.3. *Racecadotril*

Racecadotril is a derivative of benzyl ester and is used as an effective anti-diarrhea drug [85,86]. The EI mass spectrum of racecadotril is characterised by a large number of fragments and relative low abundance of molecular ion M^+. In our experiment, a suitable photon energy (8.7 eV) exclusively forms only the molecular ion at m/z 385,

Downloaded At: 15:33 21 January 2011

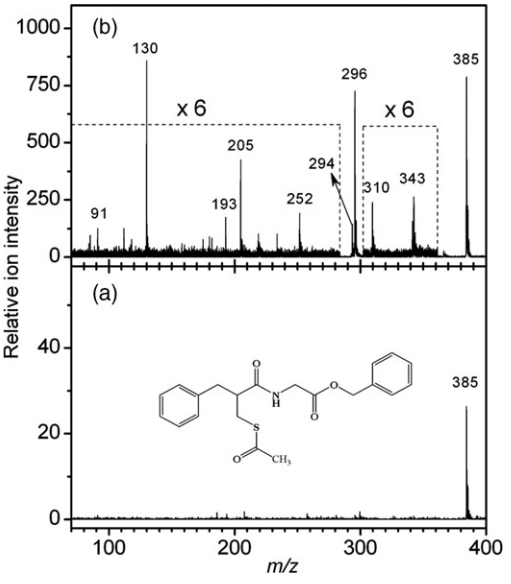

Figure 8. Photoionisation mass spectra of racecadotril at the photon energies of (a) 8.7 and (b) 10.0 eV. Part of the spectrum is amplified by a factor of 6, as labelled in the figure [55].

Downloaded At: 15:33 21 January 2011

as shown in Figure 8. Higher photon energy (10.0 eV) gives a series of fragment ions. The elimination of neutral ketene is one of the major fragmentation pathways to yield the product at m/z 343. In this pathway, C–S bond fission occurs after intermolecular hydrogen transfer. Subsequently, the loss of SH radical results in the even-electron ion at m/z 310 with a terminal $-CH{=}CH_2$ double bond. The m/z 310 ion can also be produced from M^+ by charge-induced fragmentation. At this photon energy, M^+ readily eliminates a CH_2SCOCH_3 group to produce the most abundant fragment at m/z 296. A relatively low signal at m/z 294 is reasonably attributed to the loss of a benzyl radical from M^+. The m/z 205 ion may originate from the loss of the C_7H_5 group from the m/z 294 ion, although eliminating a radical is unfavourable for most of the even-electron ions. The fragment at m/z 130 may originate from the loss of $SHCOCH_3$ from the m/z 205 ion, as demonstrated in Scheme 3.

These results prove that IR LD/VUV PIMS could be a complementary tool for the identification of drug structure and be useful in elucidating the possible fragmentation pathways.

5. Photoionisation and photodissociation studies on quinones

Quinones and their derivatives have highly carcinogenic and mutagenic properties in air particulates [87–89]. These kinds of compounds exist widely in nature; they have a variety of important characteristics for biological activities and play vital roles in biological systems [90]. The mass spectrometric analysis of quinones has been well established for several decades by GC/EI-MS [89], MALDI TOF-MS [91], ESI-MS [92–94], atmospheric pressure chemical ionisation mass spectrometry (APCI-MS)[95] and L2MS [96].

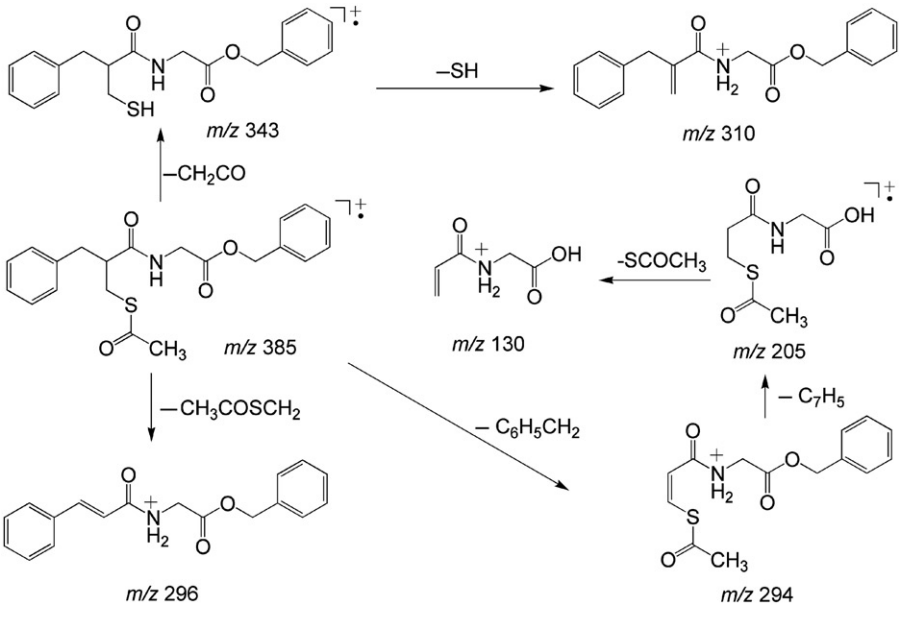

Scheme 3. Proposed fragmentation pathways for the racecadotril cation [55].

Downloaded At: 15:33 21 January 2011

We have used IR LD/VUV PIMS to study the photoionisation and photodissociation of several quinones [56,57]. The signal intensities of these series of quinones are very high with relative low laser power. The consecutive losses of two carbon monoxides from molecular ion are observed, as reported by other researchers [97,98].

5.1. *1,2-Naphthoquinone and 1,4-naphthoquinone*

The mass spectra of 1,2-naphthoquinone (1,2-NQ) at different photon energies are displayed in Figure 9. From our experiments, we found that molecular ion M^+ of 1,2-NQ can be obtained below 9.2 eV. The subsequent fragment products are $(M–CO)^+$ and $(M–C_2O_2)^+$. At a higher photon energy than 14.0 eV, fragments at m/z 76 and 63 are gradually formed, which are assigned to $(M–C_2O_2–C_2H_2)^+$ and $(M–C_2O_2–C_3H_3)^+$, respectively. The theoretical calculations tell us that the detailed fragmentation pathways are far more complex, which can be found elsewhere [57].

Between isomers 1,2-NQ and 1,4-NQ, the latter has a higher IE due to the orientation of its *para*-oxygen atoms. As can be seen from Figure 10, the major fragments of 1,4-NQ at the photon energy of 18.0 eV are m/z 130, 102 and 76 ions, which are similar to those of 1,2-NQ. Still, there are three obvious differences between the two spectra: (1) compared with that of 1,4-NQ, the relative ion intensity of 1,2-NQ molecular ion is very low. At the photon energy of 20.0 eV, the signal of 1,4-NQ molecular ion is the base peak, while the relative intensity of 1,2-NQ molecular ion is only 8% of the base peak at m/z 102, which is comparable to the result from EI MS (3.3%). This discrepancy is due to the relative low AE for the $(M–CO)^+$ from 1,2-NQ, making it more labile. In our experiments, we can

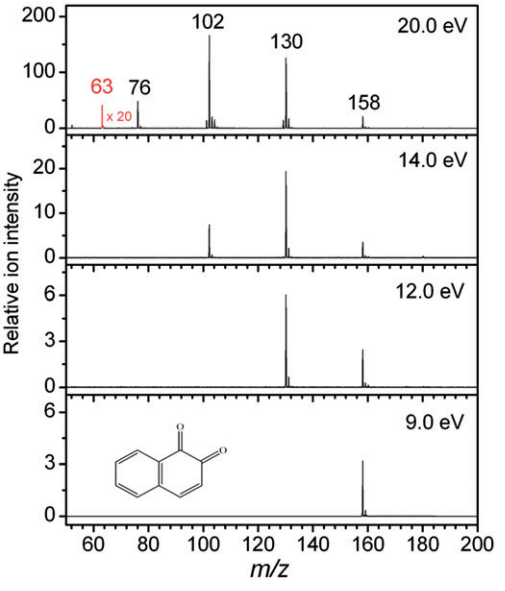

Figure 9. [Colour online]. Photoionisation mass spectra of 1,2-NQ at different photon energies [57].

Downloaded At: 15:33 21 January 2011

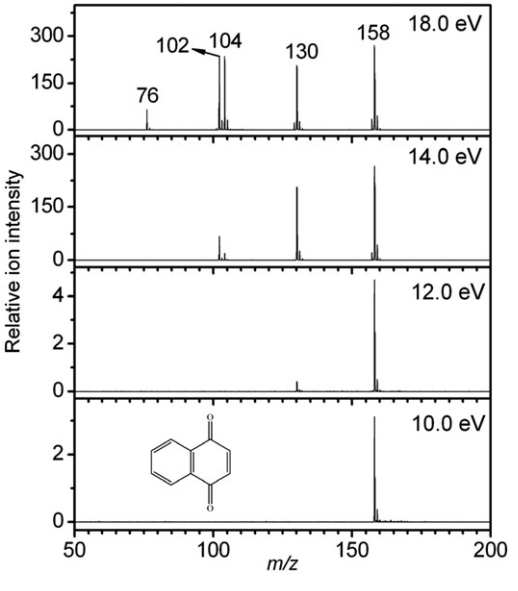

Figure 10. Photoionisation mass spectra of 1,4-NQ at different photon energies [57].

observe the appearance of $(M–CO)^+$ from 1,2-NQ at the photon energy of 9.2 eV (not the accurate AE value), which is just 0.3 eV higher than the IE value. In comparison, the detection of $(M–CO)^+$ from 1,4-NQ occurs only when the energy is increased to around 12.3 eV, which is 1.8 eV higher than the IE value; (2) the relative intensities of the m/z 104

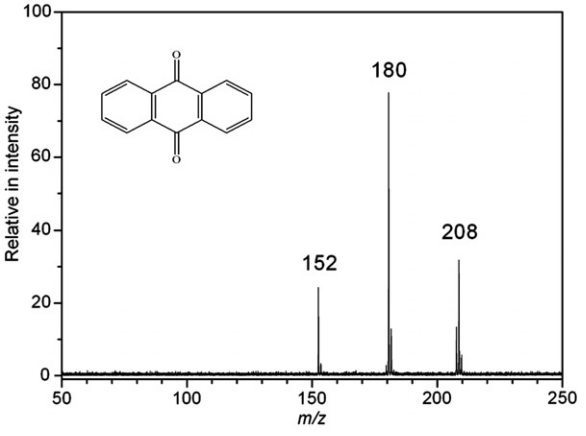

Figure 11. Photoionisation mass spectrum of 9,10-AQ at the photon energy of 16.0 eV [57].

Downloaded At: 15:33 21 January 2011

ion from 1,2-NQ and 1,4-NQ are totally different. The intense peak at m/z 104 of 1,4-NQ originates from the elimination of neutral C_2H_2 molecule after the loss of one CO group from the molecular ion, which has been reported previously [99,100]. For 1,2-NQ, however, the m/z 104 ion includes contributions from two competitive pathways, which may result in the relatively low fragmentation yield [57]; and (3) compared with that of 1,2-NQ, the m/z 63 ion from 1,4-NQ is too low to be detected even at the photon energy of 20.0 eV. The similar results are found from 70 eV EI experiments, where the relative abundance of the m/z 63 ion formed from 1,2-NQ is around fivefold larger than that from 1,4-NQ [71].

5.2. *9,10-Anthraquinone, 9,10-phenanthroquinone and benz[a]anthracene-7,12-dione*

The IE of 9,10-AQ is 9.25 eV. Thus, the molecular ion of 9,10-AQ can be clearly detected at the photon energy of 9.3 eV. Increasing the photon energy will result in the continuous decarbonylation processes to form $(M–CO)^+$ and $(M–C_2O_2)^+$ ions, as shown in Figure 11. At photon energies higher than 18.0 eV, a signal at m/z 126 is observed, which is formed via decomposition of one of the aromatic rings of *ortho*-biphenylene with the loss of C_2H_2 (not shown here) [101]. The photodissociation behaviour of 9,10-PQ is the same as that of 9,10-AQ. The $(M–CO)^+$, $(M–C_2O_2)^+$ and $(M–C_2O_2–C_2H_2)^+$ ions at m/z 208, 180 and 152 can be easily observed in the mass spectra at relatively higher photon energy [57].

The losses of CO groups from benz[a]anthracene-7,12-dione (BAD) are somewhat complicated due to its structural asymmetry. Since the loss of either C(7)O or C(12)O leads to the same peak at m/z 230, the first decarbonylation sequence cannot be unambiguously discerned from the mass spectrum. Thus, these dissociation pathways are considered and calculated with the B3LYP method. The theoretical calculations suggest that the AE of $(M–CO)^+$ from the loss of C(7)O or C(12)O is the same (10.57 eV). But the energy barriers for the loss of the second CO group to generate m/z 202 ion are slightly different, which are calculated to be 11.45 eV (loss of C(7)O) and 11.58 eV (loss of C(12)O), respectively.

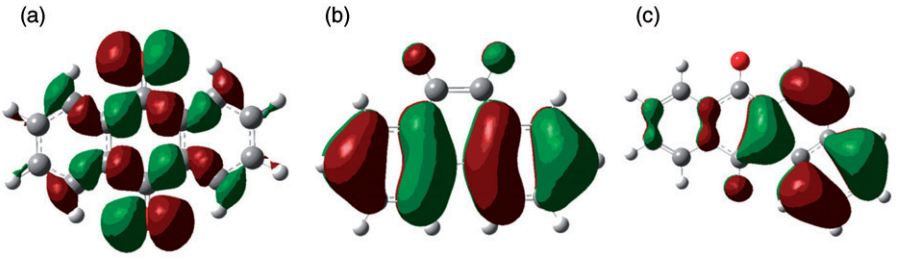

Figure 12. [Colour online]. The highest occupied molecular orbitals of (a) 9,10-AQ, (b) 9,10-PQ and (c) BAD [57].

Hence, we conclude that the sequence of the consecutive losses of CO from BAD molecular cation is not affected markedly by molecular configuration.

The PIE measurements were carried out for these compounds. The approximate IE for *para*-quinone 9,10-AQ was measured to be 9.2 eV. In 9,10-PQ, where the oxygen atoms are adjacent, ionisation is more favourable with an approximate IE of 8.6 eV. Both the values are similar to the previous results [71]. The theoretical calculations show that the highest occupied molecular orbital (HOMO) of 9,10-AQ is a 'lone pair' n MO, while for 9,10-PQ the HOMO is a 'delocalised' π MO. In BAD, affected by the additional planar benzene ring fused to 9,10-AQ, the HOMO of BAD changes from n MO to the more tightly bound π MO. Accordingly, the IE of BAD is decreased by 0.9 eV, compared to that of 9,10-AQ. The MOs of these quinones, as calculated using the B3LYP method, are shown in Figure 12.

Downloaded At: 15:33 21 January 2011

5.3. *1,8-Dihydroxyanthraquinone*

1,8-Dihydroxyanthraquinone (1,8-DHAQ) is a hydroxyl-substituted derivative of 9,10-AQ. Due to the existence of two additional hydroxyl groups, intramolecular hydrogen bonds are formed, which will influence molecular stability and induce tautomerisation via a proton transfer. Ferreiro and Rodríguez-Otero [102] demonstrated that 1,8-DHAQ in its ground state exhibits two intramolecular hydrogen bonds (O–H $\cdots$ O). Hence, the fragmentation processes of 1,8-DHAQ are very complicated. At relatively low photon energy, the mass spectrum is characterised by the presence of fragments at m/z 223, 212 and 184, which are attributed to $(M–OH)^+$, $(M–CO)^+$ and $(M–C_2O_2)^+$ ions (Figure 13). When the excitation energy is increased to 20.0 eV, more fragments are found at m/z 156, 155, 138 and 128, etc. The peak at m/z 156 corresponds to the loss of the third CO group, while the relatively weak fragment at m/z 155 is attributed to the $(M–C_3O_3H)^+$ ion. The m/z 138 ion may be due to the loss of H_2O from $(M–C_3O_3)^+$ ion or the loss of OH radical from the $(M–C_3O_3H)^+$ ion. The elimination of the fourth CO group produces the fragment of $(M–C_4O_4)^+$ at m/z 128. For comparison, the mass spectrum with 70.0 eV EI ionisation is shown in Figure 13(e) [71]. Due to the presence of intramolecular hydrogen bonds, detailed dissociation channels cannot be deduced by the mass spectra alone. For example, the elimination of carbon monoxide can occur from the carbonyl group or C–O(H) group of hydroxyanthraquinones. Thus, calculations are introduced to give a clearer picture. The calculated results at the B3LYP/6-31+G(d) level

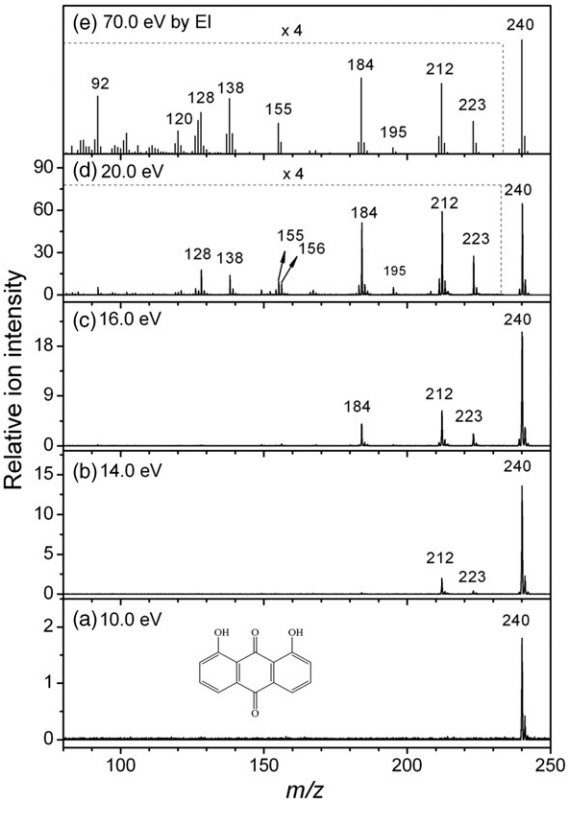

Figure 13. Photoionisation mass spectrum of 1,8-DHAQ at different photon energies [56].

Downloaded At: 15:33 21 January 2011

show five lowest-energy structures of isomeric 1,8-DHAQ radical cations upon ionisation, as shown in Figure 14. Each one of them can undergo bond fission and fragmentation via a series of transition states (TSs) with various barriers, as described previously [56].

6. Photoionisation and photodissociation studies on amino acids

Amino acids are the most important building blocks of life, and they play key roles in the origin of life on the earth [103,104]. As photoionisation and photodissociation processes in the VUV range are related to molecular radiation damage, relevant investigations in the gas phase are worthwhile endeavors [23,105–107].

α-Alanine, β-alanine and sarcosine are isomers with the molecular weight of 89. Here, we present parts of the photoionisation and photodissociation results studied by IR VUV/PIMS and theoretical calculations. The detailed discussion can be found in the previous reports [52,53].

6.1. α-*Alanine*

Among the 20 natural found amino acids, α-alanine is the first chiral compound with a distinct enantiomeric structure. A rich variety of conformers of α-alanine are found arising

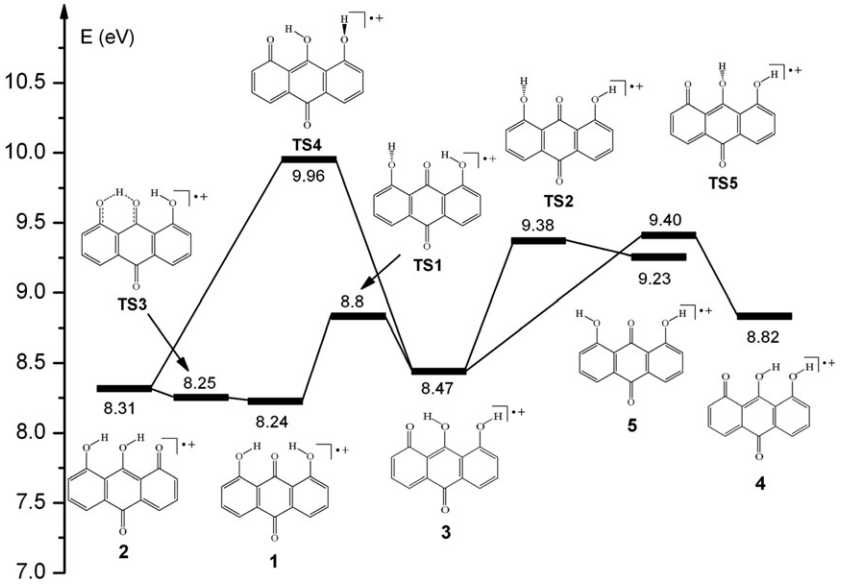

Figure 14. Energy profiles for interconversion between five isomeric 1,8-DHAQ cations. All the energies (in eV) are relative to that of neutral 1,8-DHAQ [56].

Downloaded At: 15:33 21 January 2011

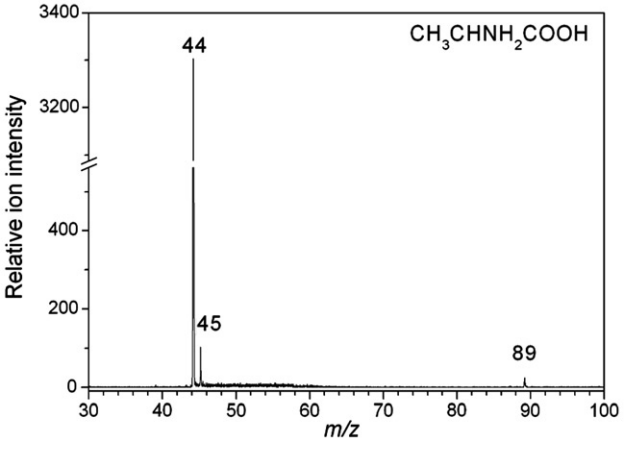

Figure 15. Photoionisation mass spectrum of α-alanine at the photon energy of 10.0 eV [52].

from various types of intramolecular hydrogen-bonding (IHB) [108]. Jochims *et al.* [20] have investigated α-alanine by PIMS in the photon energy range of 6–22 eV. They showed that major fragments of α-alanine below 13.6 eV are at m/z 44, 42, 28 and 18. In our work, a relatively low photon energy of 10.0 eV is selected, and only the nascent fragments at m/z 44 and 45 are studied and discussed in detail. As demonstrated in Figure 15 [52], the fragment at m/z 44 is the base peak with the highest abundance, which is attributed to

the $CH_3CHNH_2^+$ ion. It is formed from the simple C–C(O) bond fission accompanied by losing the COOH fragment. The ion at m/z 45 can be assigned to $CH_3CHNH_3^+$. The theoretical calculations indicate this ion is formed from the intramolecular hydrogen transfer and subsequent decarboxylation process. The fragment at m/z 45 can also be assigned to $COOH^+$ which is formed by the simple rupture of the central C–C bond [20]. Three competitive formation pathways for these fragments are depicted below [52]:

$$NH_2CHCH_3COOH^+ \rightarrow CH_3CHNH_2^+ + COOH \quad (1)$$

$$NH_2CHCH_3COOH^+ \rightarrow CH_3CHNH_3^+ + CO_2 \quad (2)$$

$$NH_2CHCH_3COOH^+ \rightarrow CH_3CHNH_2 + COOH^+. \quad (3)$$

Five stable conformers of α-alanine including three kinds of IHB (N–H $\cdots$ O, N–H $\cdots$ O(H) and O–H $\cdots$ N) are considered at the B3LYP/6-31++G(3df,2p) and G3B3 levels. The formation channels from the five conformers to the fragment ions were calculated. The relative energies of TSs and intermediates (INTs) are obtained. We have shown that at the photon energy of 10.0 eV, the m/z 44 ion can only be assigned to $CH_3CHNH_2^+$. The theoretical AE value for this fragment is determined to be 9.61 eV at the G3B3 level. Experimentally, we also find that at around 9.5 eV, the m/z 44 could be gradually observed. In comparison, $COOH^+$ has a theoretical AE of 11.79 eV, indicating it is the second product ion at m/z 45 from the decomposition of molecular ion.

The thermodynamical or kinetic priorities at the photon energy of 10.0 eV are considered for $CH_3CHNH_2^+$ and $CH_3CHNH_3^+$. We conclude that the formation of the $CH_3CHNH_2^+$ ion is kinetically favoured, as the appearance of $CH_3CHNH_3^+$ via hydrogen transfer and subsequent decarboxylation needs to overcome a higher barrier than that of $CH_3CHNH_2^+$ via direct bond fission. However, when the energies of the reactions are considered, the situation is different. We found that the total energy of $CH_3CHNH_3^+$ and CO_2 is lower than that of $CH_3CHNH_2^+$ and COOH. Therefore, the formation of $CH_3CHNH_3^+$ is thermodynamically favoured. The stronger signal at m/z 44 suggests that the kinetic factor is predominant in controlling the rearrangement and reaction of the α-alanine cation [52]. In addition, the direct dissociation pathways which produce radicals are found to be entropically favoured, as reported by Deleuze and coworkers [109,110].

6.2. *β-Alanine*

β-Alanine, the simplest β-amino acid, is found to be the most abundant of the amino acids identified in carbonaceous meteorites [111]. Due to the molecular flexibility, many low-lying torsional conformers have been found in the gas phase by experimental and computational methods [112–114], and at least three *gauche* (G) conformers and one *anti* (A) conformer were found to coexist in the gas phase [112].

As shown in Figure 16, the major fragments at m/z 45, 44, 43 and 18, in addition to the molecular ion, are observed at the photon energy of 12.0 eV with IR LD/VUV PIMS [53]. The previous studies have proposed to assign the fragment at m/z 45 to $COOH^+$ [20]. Based on G3B3 calculations, the AE value of $COOH^+$ from a direct C–C bond cleavage is 11.8 eV. However, the m/z 45 ion can be detected at around 9.3 eV, much lower than

Downloaded At: 15:33 21 January 2011

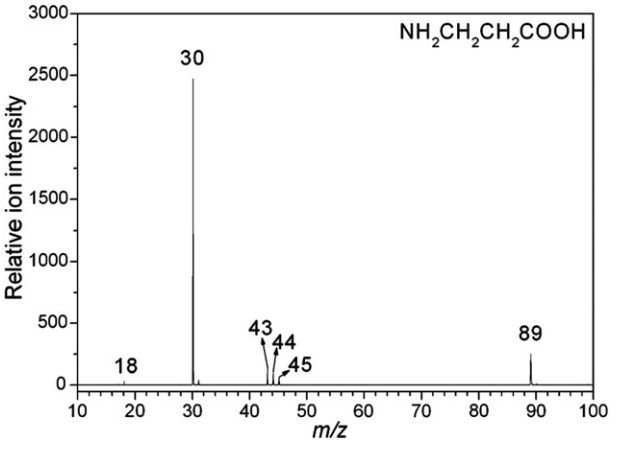

Figure 16. Photoionisation mass spectrum of β-alanine at the photon energy of 12.0 eV [53].

Downloaded At: 15:33 21 January 2011

11.8 eV. Therefore, we attribute this fragment to $NH_3CH_2CH_2^+$ instead, a product formed by intramolecular hydrogen transfer and subsequent decarboxylation of a *gauche* conformer (G2) of β-alanine, with a G3B3 AE of 9.2 eV.

The computational results reveal that the fragment at m/z 43 may well be $NH_2CHCH_2^+$, because this cation is the most stable isomer on the $C_2H_5N^+$ cationic surface. It can be formed from *gauche* and *anti* conformers via several successive elimination processes. The detailed decomposition pathways are depicted below [53]:

$$NH_2CH_2CH_2COOH^+(G1+) \rightarrow NH_2CHCH_2^+ + HCOOH \quad (4)$$

$$NH_2CH_2CH_2COOH^+(G1+) \rightarrow NH_2CHCH_2^+ + CO + H_2O \quad (5)$$

$$NH_3CH_2CH_2COO^+(G2+) \rightarrow NH_2CHCH_2^+ + H_2 + CO_2 \quad (6)$$

$$NH_2CH_2CH_2COOH^+(A+) \rightarrow NH_2CHCH_2^+ + CO + H_2O. \quad (7)$$

Compared with the signal intensity of m/z 44 from α-alanine, that for β-alanine is extremely low. We assign this fragment to $NH_2CHCH_3^+$ rather than $NH_2CH_2CH_2^+$ ion, because the calculations predict that the former ion is more stable than the latter (via direct bond dissociation) by 2.6 eV. The fragmentation pathway may be predicted as: one *gauche* conformer undergoes a 1,2-hydrogen transfer forming $NH_2CHCH_3COOH^+$, immediately followed by the fission of the C–C bond, yielding $NH_2CHCH_3^+$ and COOH radical. The fragment ion at m/z 30 is attributed to $NH_2CH_2^+$ via the direct loss of a CH_2COOH radical [20]. Similar to that of glycine [71], the $NH_2CH_2^+$ ion has the strongest ion intensity, which is mainly due to the delocalisation of the lone-pair electrons along the C–N bond, making this fragment extremely stable. This observation is similar to the previous results using photoionisation [111] and EI [71] methods. In the case of the m/z 18 ion, it can be reasonably assigned to NH_4^+ [20], which may originate from $NH_3CH_2CH_2^+$ after one hydrogen atom is transferred from carbon atom to nitrogen atom and subsequent N–C bond cleavage.

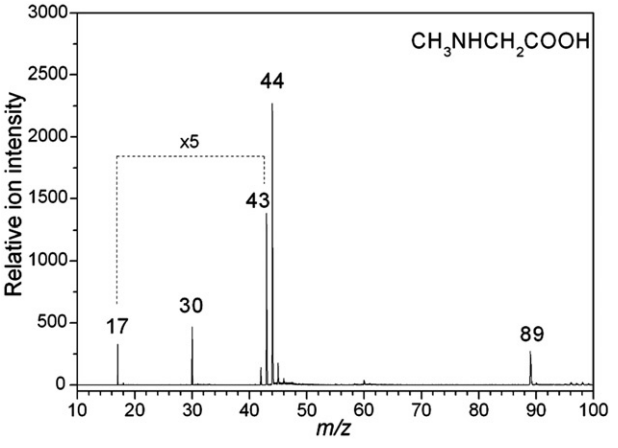

Figure 17. Photoionisation mass spectrum of sarcosine at the photon energy of 12.0 eV [116].

Downloaded At: 15:33 21 January 2011

6.3. *Sarcosine*

Sarcosine belongs to the family of secondary amino acids. Under monomeric oxidase, it can be oxidised to yield glycine and formaldehyde by demethylation [115]. Many stable conformers for sarcosine have been proposed, among which the conformer with the N–H···O=C intramolecular hydrogen bond and the *cis* carboxylic group is the most stable one. The photoionisation and photodissociation mass spectra of sarcosine at different photon energies were measured. As shown in Figure 17, a series of fragments at m/z 30, 42, 43, 44, 45 as well as the molecular ion are formed at the excitation energy of 12.0 eV [116].

The highest ion signal at m/z 44 is attributed to $CH_3NHCH_2^+$, arising from the direct rupture of the C–C bond. The intramolecular hydrogen transfer followed by decarboxylation is also found for sarcosine, forming the fragment at m/z 45 with a relative low intensity. The product ion at m/z 43 can be attributed to $CH_2NHCH_2^+$ with two proposed formation pathways [116]. As in the mass spectra of glycine and β-alanine, sarcosine also gives a product ion at m/z 30. This ion corresponds to $NH_2CH_2^+$, which comes from a series of hydrogen transfer and bond rupture processes.

7. Photoionisation and photodissociation studies on cholesterol

Cholesterol is a precursor of steroid hormones and bile acids, and acts as a major structural component of plasma membranes [117,118]. Many mass spectrometry-based methodologies have been attempted for the analysis of cholesterol [119,120]. However, due to the low ion yield and unsatisfactory sensitivity, derivatisation is needed before mass spectrometric analysis [121,122].

We have studied the photoionisation mass spectra of cholesterol with IR LD/VUV PIMS [54]. At the photon energy of 10.0 eV, the pure molecular ion at m/z 386 is observed with high intensity. By increasing photon energy to 12.0 eV, many fragments are formed, as shown in Figure 18 [54]. The decomposition of cholesterol and its derivatives is complex

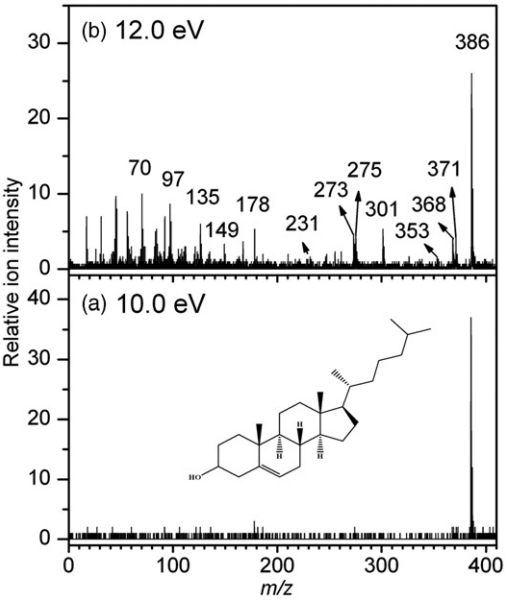

Figure 18. Photoionisation mass spectrum of cholesterol at different photon energies [54].

Downloaded At: 15:33 21 January 2011

due to the complexity of the pathways involving dehydration, ring cleavage, side-chain cleavage and so on [119,123]. In order to obtain a better understanding of the photo-induced dissociative reactions, B3LYP calculations were carried out to clarify the fragmentation mechanisms [54].

We find that dehydration is a major process upon ionisation. The theoretical calculations indicate that M^+ can undergoes C4–H and C3–O(H) bond fissions via a TS with a four-membered ring to form the fragment at m/z 368 and H_2O, as shown in Scheme 4. Further side-chain cleavage on the C17–C20 bond of the m/z 368 ion will produce the m/z 255 ion, while direct bond cleavage of M^+ will result in the fragment at m/z 273. From another side-chain cleavage, the fragment ion at m/z 371 is formed via C25–C26 or C25–C27 bond fission to lose a CH_3 radical from M^+. The m/z 353 ion is attributed to the consecutive loss of H_2O and CH_3. The m/z 301 ion may come from the contribution of C22–C23 bond cleavage. Based on theoretical calculations, this direct dealkylation channel has the lowest energy barrier. To gain stability, it is found that the C13–C17 bond of the m/z 301(a) ion is indeed broken [123]. In addition, ring-opening after dehydration is another possible decomposition channel [54]. The loss of C_7H_9 after dehydration and subsequent ring-opening results in the fragment at m/z 275. The calculations suggest that a series of TSs and INTs are involved to form this ion. In addition, the formation of the fragment at m/z 231 also involves several TSs and INTs. Further ejection of C_4H_5 from the m/z 231 ion yields the ion at m/z 178. Actually, the m/z 178 ion has three isomeric structures (labelled (a)−(c)), which can convert between each other via different TSs. Furthermore, after C-ring cleavage the m/z 178 ion can also be formed from the m/z 301 ion. The detailed fragmentation pathways along with relative energies of TSs and INTs can be found in our previous work [54].

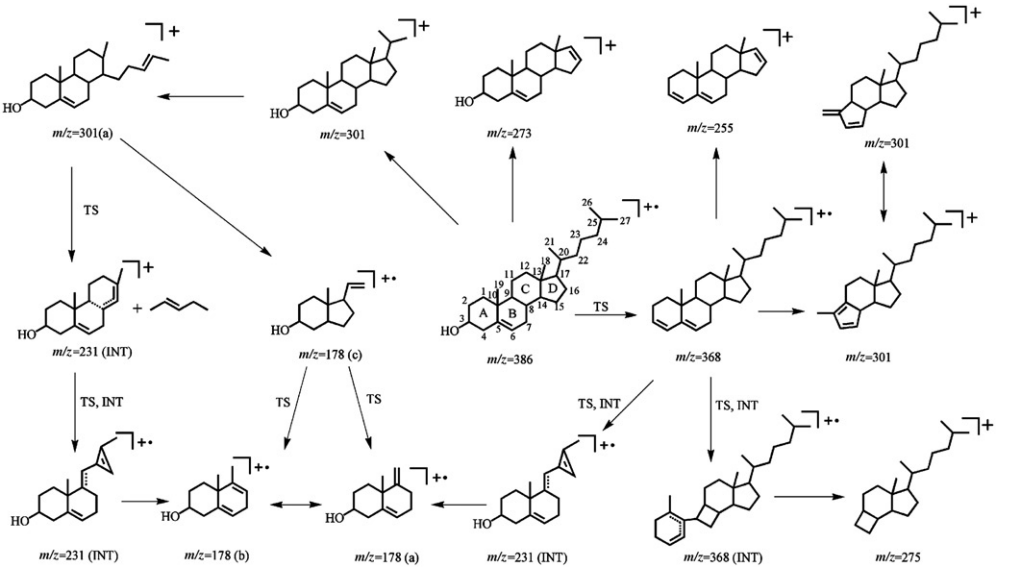

Scheme 4. Proposed fragmentation pathways for the cholesterol cation [54].

Downloaded At: 15:33 21 January 2011

8. Application on the identification of mixtures

8.1. *Simple mixtures*

The characterisation of the organic molecular structures of complex mixtures, such as natural products and oils, is a big challenge because of their complicated physical and chemical properties. Typically, preliminary gas/liquid chromatographic separation is implemented before the mass spectrometric analysis. To obtain reliable results, complex pretreatment and derivatisation are crucial. L2MS has also been attempted to analyse the components in organic mixtures, such as interplanetary dust particles and meteorites, in which a series of PAHs were identified directly [44–46].

By virtue of the wide tunability in the VUV range from synchrotron, nearly all the organic molecules can be ionised, making IR LD/VUV PIMS a complementary tool for the identification of chemical mixtures. At a selective photon energy which is slightly higher than the IEs of all analytes, a mass spectrum could be obtained with the information of mass and controllable fragments. We have attempted to use a photon energy of 9.5 eV on a six-quinone mixture, including 1,4-NQ (m/z 158, IE = 9.5 eV [71]), 1,2-acenaphthylenedione (AND) (m/z 182, IE = ~8.7 eV [71]), 9,10-AQ (m/z 208, IE = 9.25 eV [71]), 9,10-PQ (m/z 208, IE = 8.64 eV [71]), DHAQ (m/z 240, IE = 8.5 eV [56]) and BAD (m/z 258, IE = 8.3 eV [57]). As shown in Figure 19, five peaks of molecular ions are clearly distinguished from the mass spectrum, while no fragments are observed. The ion at m/z 208 comes from the contribution from two isomers, 9,10-AQ and 9,10-PQ. As the IE difference of these two isomers is relatively large, PIE measurement can be applied to identify them, as shown in the inset of Figure 19.

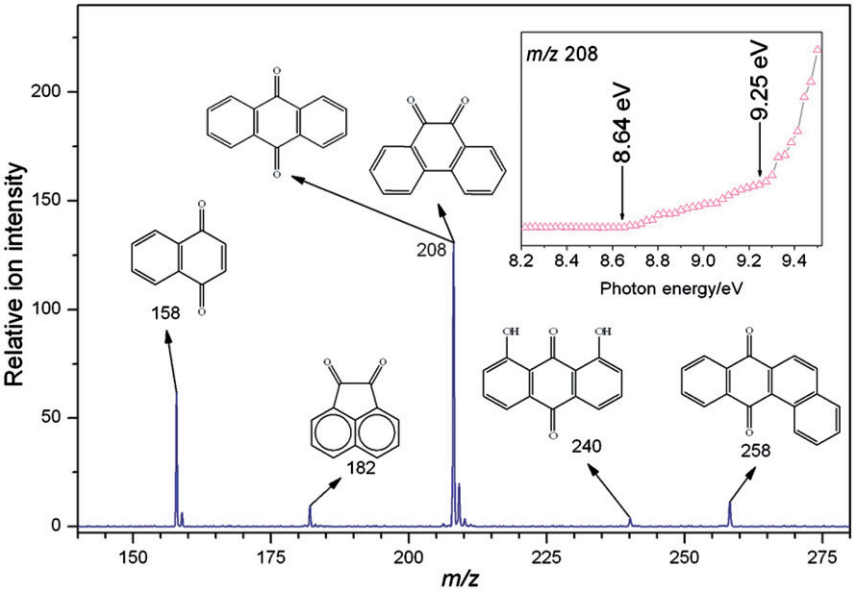

Figure 19. [Colour online]. Photoionisation mass spectrum of a quinone mixture containing 1,4-NQ (*m*/*z* 158), AND (*m*/*z* 182), 9,10-AQ (*m*/*z* 208), 9,10-PQ (*m*/*z* 208), 1,8-DHAQ (*m*/*z* 240) and BAD (*m*/*z* 258) at the VUV photon energy of 9.5 eV. The inset shows the PIE spectrum of a mixture of 9,10-AQ (*m*/*z* 208) and 9,10-PQ (*m*/*z* 208) [49].

Downloaded At: 15:33 21 January 2011

8.2. *Heavy oils*

Heavy oil, a more complex mixture was also introduced into our experiment [58]. To date, numerous experimental methods have been utilised to measure the molecular weight distribution of heavy oil, from which the mean molecular weight can be deduced. However, pronounced controversy arose from these different techniques [124–129]. We measured the photoionisation mass spectra of four samples of heavy oil using IR LD/VUV PIMS at the photon energy of 9.8 eV [58], and typical peaks of hydrocarbon in saturates were observed. As demonstrated in Figure 20, each sample displays a broad distribution of ions, in which the carbon number ranges from 15 to 30. These dominant peaks are assigned to seven classes of saturated hydrocarbons: chain C_nH_{2n+2}, monocyclic C_nH_{2n}, bicyclic C_nH_{2n-2}, tricyclic C_nH_{2n-4}, tetracyclic C_nH_{2n-6}, pentacyclic C_nH_{2n-8} and hexacyclic C_nH_{2n-10}. The relative intensities for the peaks of various classes are sample-dependant, due to the different sample preparation processes. Owing to the 'soft' SPI, only minor fragments below *m*/*z* 200 with relatively low intensities are detected. Actually, these additional fragmentation processes of the samples can be markedly reduced by carefully tuning the photon energy.

Figure 21 shows the photoionisation mass spectra of sample 2 at various photon energies. At the low energy of 9.0 eV, aside from the predominant molecular ions of hydrocarbons, only negligible fragments are seen. With the increase of photon energy, an enormous array of fragment ions is produced in the mass range of 80–200, accompanied by a decrease of relative intensities for the high molecular weight ions.

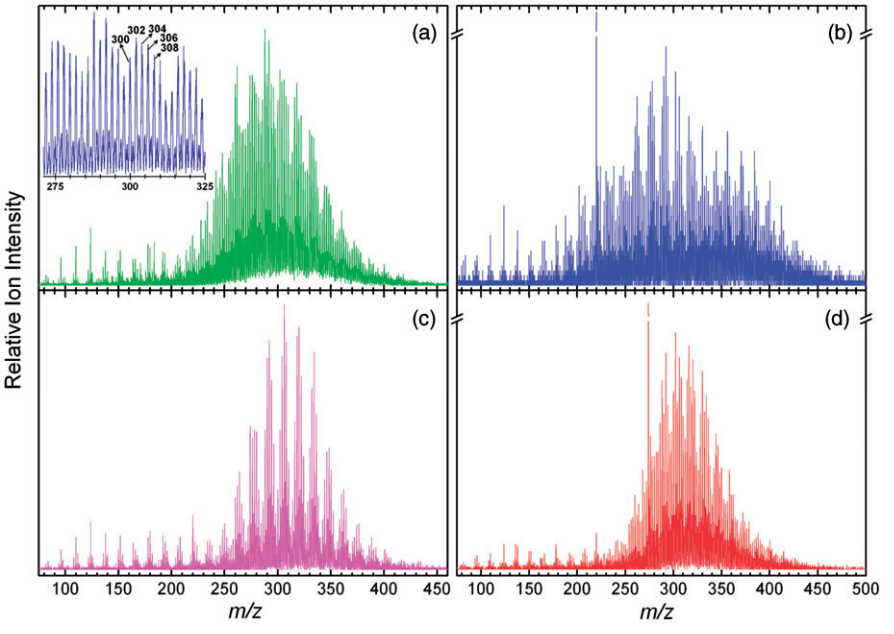

Figure 20. [Colour online]. Photoionisation mass spectra of four different samples measured at the VUV photon energy of 9.80 eV [58]: (a) sample 1, (b) sample 2, (c) sample 3 and (d) sample 4. An inserted figure of (a) clearly displays the peaks with even masses. IR laser power was set at ~6 mJ/pulse. Each spectrum was recorded for a period of 100 s.

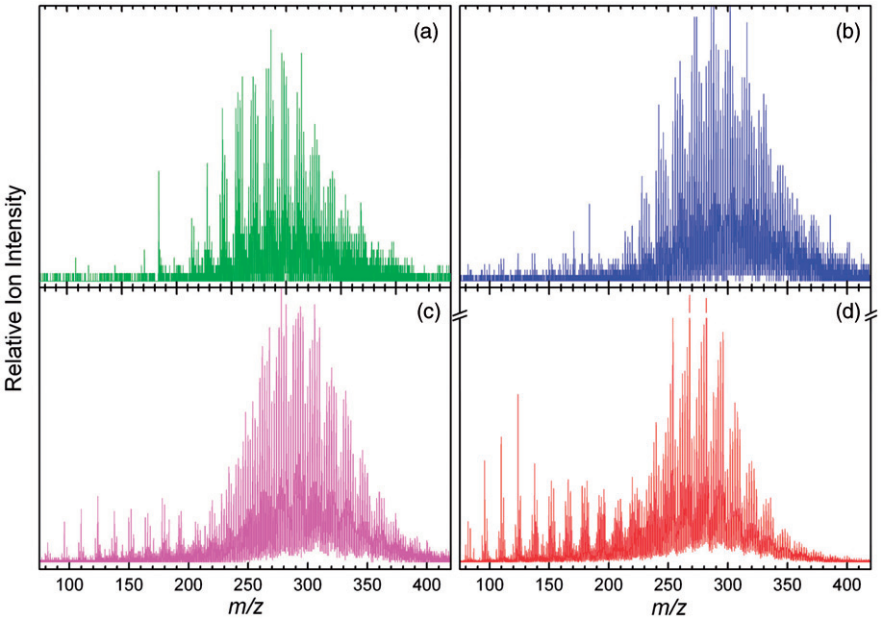

Figure 21. [Colour online]. Photoionisation mass spectra of sample 1 obtained with four different photon energies of (a) 9.00 (b) 9.50 (c) 10.00 and (d) 10.80 eV. Each spectrum was recorded for a period of 50 s [58].

Downloaded At: 15:33 21 January 2011

The method of IR LD/VUV PIMS in the analysis of heavy oil is clearly very promising. However, the accurate identification of individual molecular structures is still a great challenge, due to the complex isomers of hydrocarbons in petroleum residues.

9. Conclusions and outlook

The aim of this review is to present a methodology combining IR laser desorption with synchrotron VUV photoionisation mass spectrometry and its applications in understanding the photoionisation and photodissociation processes and fragmentation processes of nonvolatile organic molecules. A large variety of organic molecules such as amino acids, steroids, drugs, quinones, DNA bases and complex mixtures have been investigated. Due to the high energy resolution of synchrotron radiation, the fragments of the analyte can be gradually formed with the increase of photon energies. As the analytes are rotationally and vibrationally hot, only rough IEs with relatively high uncertainties are obtained according to the observable onsets. To complement the experimental work, *ab initio* calculations were carried out using the Gaussian 03 program. The B3LYP method using several different base sets was used to optimise structures and calculate relative energies of neutrals, ions, TSs and INTs. With the help of the theoretical results, the fragmentation pathways of molecules can be deduced with reliable structural and energetic results. Some potential competitive channels can be differentiated and possible reasons for the formation of some ambiguous products are proposed.

The experimental results demonstrate that with selected IR laser power and ionisation photon energy, exclusive molecular ions can be formed by virtue of near-threshold SPI. This advantage makes IR LD/VUV PIMS a complementary tool for the identification of chemical mixtures, particularly for natural products without preliminary chromatographic separation. It has been suggested that IEs can be estimated by measuring the PIE spectra. Although these data have not been corrected, they are still usable in discriminating some mixtures, or even isomers. In addition, with the improvements of mass resolution, mass range, detection sensitivity and instrumental stability, IR LD/VUV PIMS may well be a candidate of imaging mass spectrometry, which is used to probe the chemical organisation of a sample and their spatial distribution *in situ*, similar to the usage of secondary ion mass spectrometry (SIMS) and MALDI imaging of biological samples.

Moreover, the method can also be improved to obtain the accurate fundamental thermodynamic data, including IEs, AEs, bond dissociation energies and so on. The crucial aspect here is to introduce the samples into high-vacuum chamber via jet cooling so as to reduce the internal energy. In summary, despite the inconvenience of using synchrotron radiation, the results in this study have demonstrated the promising applications of IR LD/VUV PIMS in the photoionisation and photodissociation studies on nonvolatile organic molecules.

Downloaded At: 15:33 21 January 2011

Acknowledgements

We thank Professor Wai-Kee Li from the Chinese University of Hong Kong and Dr Christopher J. Bennett from University of Hawaii for useful discussions. This work has been supported by the grants from Chinese Academy of Sciences (YZ200764), the Natural Science Foundation of China (10705026, 10979043 and 10805047), the Ministry of Science and Technology of China

(2007DFA61310), National Basic Research Program of China (973) (2007CB815204) and Special Grade of the Financial Support from China Postdoctoral Science Foundation (200801223).

References

[1] R. A. Bingham and P. L. Salter, Anal. Chem. **48**, 1735 (1976).
[2] H. Hertz, Ann. Phys. Chem. **31**, 983 (1887).
[3] V. Schmidt, Rep. Prog. Phys. **55**, 1483 (1992).
[4] S. T. Pratt, Rep. Prog. Phys. **58**, 821 (1995).
[5] H. Kjeldsen, J. Phys. B: At. Mol. Opt. Phys. **39**, R325 (2006).
[6] F. L. Mohler and C. Boeckner, Phys. Rev. **28**, 46 (1926).
[7] J. Berkowitz, Photoabsorption, *Photoionization and Photoelectron Spectroscopy* (Academic Press, New York, 1979).
[8] K. Watanabe, F. F. Marmo, and E. C. Y. Inn, Phys. Rev. **91**, 1155 (1953).
[9] K. Watanabe, J. Chem. Phys. **22**, 1564 (1954).
[10] W. C. Walker and G. L. Weissler, J. Chem. Phys. **23**, 1962 (1955).
[11] N. Wainfan, W. C. Walker, and G. L. Weissler, J. Appl. Phys. **24**, 1318 (1953).
[12] F. P. Lossing and I. Tanaka, J. Chem. Phys. **25**, 1031 (1956).
[13] H. Hurzeler, M. G. Inghram, and J. D. Morrison, J. Chem. Phys. **28**, 76 (1957).
[14] C. Y. Ng, Int. J. Mass Spectrom. **200**, 357 (2000).
[15] J. Wang, Y. Y. Li, T. C. Zhang, Z. Y. Tian, B. Yang, K. W. Zhang, F. Qi, A. G. Zhu, Z. F. Cui, and C. Y. Ng, Astrophys. J. **676**, 416 (2008).
[16] B. Yang, P. Oβwald, Y. Y. Li, J. Wang, L. X. Wei, Z. Y. Tian, F. Qi, and K. Kohse-Höinghaus, Combust. Flame **148**, 198 (2007).
[17] C. A. Taatjes, N. Hansen, D. L. Osborn, K. Kohse-Höinghaus, T. A. Cool, and P. R. Westmoreland, Phys. Chem. Chem. Phys. **10**, 20 (2008).
[18] H. W. Jochims, M. Schwell, H. Baumgärtel, and S. Leach, Chem. Phys. **314**, 263 (2005).
[19] M. Schwell, H. W. Jochims, H. Baumgartel, and S. Leach, Chem. Phys. **353**, 145 (2008).
[20] H. W. Jochims, M. Schwell, J. L. Chotin, M. Clemino, F. Dulieu, H. Baumgärtel, and S. Leach, Chem. Phys. **298**, 279 (2004).
[21] J. Li, J. H. Cai, T. Yuan, H. J. Guo, and F. Qi, Rapid Commun. Mass Spectrom. **23**, 1269 (2009).
[22] K. R. Wilson, L. Belau, C. Nicolas, M. Jimenez-Cruz, S. R. Leone, and M. Ahmed, Int. J. Mass Spectrom. **249–250**, 155 (2006).
[23] K. R. Wilson, M. Jimenez-Cruz, C. Nicolas, L. Belau, S. R. Leone, and M. Ahmed, J. Phys. Chem. A. **110**, 2106 (2006).
[24] Z. Yang, T. C. Zhang, Y. Pan, X. Hong, Z. C. Tang, and F. Qi, J. Am. Soc. Mass Spectrom. **20**, 430 (2009).
[25] N. C. Fenner and N. R. Daly, Rev. Sci. Instrum. **37**, 1068 (1966).
[26] R. H. Scott, P. F. S. Jackson, and A. Strasheim, Nature **232**, 623 (1971).
[27] M. A. Posthumus, P. G. Kistemaker, H. L. C. Meuzelaar, and M. C. Ten Noever de Brauw, Anal. Chem. **50**, 985 (1978).
[28] R. A. Dotter, C. H. Smith, M. K. Young, P. B. Kelly, A. D. Jones, E. M. McCauley, and D. P. Y. Chang, Anal. Chem. **68**, 2319 (1996).
[29] R. Nitsche, R. Kaufmann, F. Hillenkamp, E. Unsold, H. Vogt, and R. Wechsung, Isr. J. Chem. **17**, 181 (1978).
[30] D. M. Hercules, R. J. Day, K. Balasanmugam, T. A. Dang, and C. P. Li, Anal. Chem. **54**, 280A (1982).
[31] R. J. Vasbla and A. J. Pirona, Adv. Mass Spectrom. **4**, 107 (1968).

Downloaded At: 15:33 21 January 2011

[32] L. Cao, F. Mühlberger, T. Adam, T. Streibel, H. Z. Wang, A. Kettrup, and R. Zimmermann, Anal. Chem. **75**, 5639 (2003).
[33] J. Grotemeyer and E. W. Schlag, Angew. Chem. **100**, 461 (1988).
[34] O. P. Haefliger and R. Zenobi, Anal. Chem. **70**, 2660 (1998).
[35] T. Ferge, F. Müehlberger, and R. Zimmermann, Anal. Chem. **77**, 4528 (2005).
[36] C. Emmenegger, M. Kalberer, B. Morrical, and R. Zenobi, Anal. Chem. **75**, 4508 (2003).
[37] J. L. Trevor, K. R. Lykke, M. J. Pellin, and L. Hanley, Langmuir **14**, 1664 (1998).
[38] E. Nir, H. E. Hunziker, and M. S . de Vries, Anal. Chem. **71**, 1674 (1999).
[39] M. Kalberer, B. D. Morrical, M. Sax, and R. Zenobi, Anal. Chem. **74**, 3492 (2002).
[40] Q. Zhan, R. Zenobi, P. R. Buseck, and S. Teerman, Energy Fuels **11**, 144 (1997).
[41] Y. F. Chen, M. C. Sullards, T. T. Hoang, S. W. May, and T. M. Orlando, Anal. Chem. **78**, 8386 (2006).
[42] P. D. Edirisinghe, J. F. Moore, K. A. Skinner-Nemec, C. Lindberg, C. S. Giometti, I. V. Veryovkin, J. E. Hunt, M. J. Pellin, and L. Hanley, Anal. Chem. **79**, 508 (2007).
[43] J. L. Fye, H. H. Nelson, R. L. Mowery, A. P. Baronavski, and J. H. Callahan, Anal. Chem. **74**, 3019 (2002).
[44] J. H. Hahn, R. Zenobi, J. L. Bada, and R. N. Zare, Science **239**, 1523 (1988).
[45] S. J. Clemett, C. R. Maechling, R. N. Zare, P. D. Swan, and R. M. Walker, Science **262**, 721 (1993).
[46] M. K. Spencer, M. R. Hammond, and R. N. Zare, Proc. Natl. Acad. Sci. USA **105**, 18096 (2008).
[47] K. Tanaka, H. Waki, Y. Ido, S. Akita, Y. Yoshida, and T. Yoshida, Rapid Commun. Mass Spectrom. **2**, 151 (1988).
[48] J. Gross and K. Strupat, Trends Anal. Chem. **17**, 470 (1998).
[49] Y. Pan, T. C. Zhang, X. Hong, Y. W. Zhang, L. S. Sheng, and F. Qi, Rapid Commun. Mass Spectrom. **22**, 1619 (2008).
[50] R. B. Hall, J. Phys. Chem. **91**, 1007 (1987).
[51] G. Rhodes, R. B. Opsal, J. T. Meek, and J. P. Reilly, Anal. Chem. **55**, 280 (1983).
[52] Y. Pan, L. D. Zhang, T. C. Zhang, H. J. Guo, X. Hong, L. S. Sheng, and F. Qi, Phys. Chem. Chem. Phys. **11**, 1189 (2009).
[53] L. D. Zhang, Y. Pan, H. J. Guo, T. C. Zhang, L. S. Sheng, F. Qi, P. K. Lo, and K. C. Lau, J. Phys. Chem. A **113**, 5838 (2009).
[54] Y. Pan, L. D. Zhang, H. J. Guo, and F. Qi, Chin. J. Chem. Phys. **22**, 129 (2009).
[55] Y. Pan, H. Yin, T. C. Zhang, H. J. Guo, L. S. Sheng, and F. Qi, Rapid Commun. Mass Spectrom. **22**, 2515 (2008).
[56] Y. Pan, L. D. Zhang, H. J. Guo, and F. Qi, J. Phys. Chem. A. **112**, 10977 (2008).
[57] Y. Pan, T. C. Zhang, H. J. Guo, X. Hong, and F. Qi, J. Mass Spectrom. **43**, 1701 (2008).
[58] W. Y. Guo, Y. C. Bi, H. J. Guo, Y. Pan, F. Qi, W. A. Deng, and H. H. Shan, Rapid Commun. Mass Spectrom. **22**, 4025 (2008).
[59] S. Ptasińska, P. Candori, S. Denifl, S. Yoon, V. Grill, P. Scheier, and T. D. Märk, Chem. Phys. Lett. **409**, 270 (2005).
[60] D. Schröder, J. Loos, R. Thissen, O. Dutuit, P. Mourgues, H. E. Audier, C. Lifshitz, and H. Schwarz, Angew. Chem. Int. Ed. **41**, 2748 (2002).
[61] T. A. Cool, K. Nakajima, T. A. Mostefaoui, F. Qi, A. Mcllroy, P. R. Westmoreland, M. E. Law, L. Poisson, D. S. Peterka, and M. Ahmed, J. Chem. Phys. **119**, 8356 (2003).
[62] C. A. Taatjes, N. Hansen, A. Mcllroy, J. A. Miller, J. P. Senosiain, S. J. Klippenstein, F. Qi, L. Sheng, Y. Zhang, T. A. Cool, J. Wang, P. R. Westmoreland, M. E. Law, T. Kasper, and K. Kohse-Höinghaus, Science **308**, 1887 (2005).
[63] C. Q. Huang, B. Yang, R. Yang, J. Wang, L. X. Wei, X. B. Shan, L. S. Sheng, Y. W. Zhang, and F. Qi, Rev. Sci. Instrum. **76**, 126108 (2005).

Downloaded At: 15:33 21 January 2011

[64] F. Qi, R. Yang, B. Yang, C. Q. Huang, L. X. Wei, J. Wang, L. S. Sheng, and Y. W. Zhang, Rev. Sci. Instrum. **77**, 084101 (2006).
[65] A. G. Baboul, L. A. Curtiss, P. C. Redfern, and K. Raghavachari, J. Chem. Phys. **110**, 7650 (1999).
[66] M. J. Frisch, G. W. Trucks, H. B. Schlegel, G. E. Scuseria, M. A. Robb, J. R. Cheeseman, V. G. Zakrzewski, J. A. Montgomery, R. E. S. Jr, J. C. Burant, S. Dapprich, J. M. Millam, A. D. Daniels, K. N. Kudin, M. C. Strain, O. Farkas, J. Tomasi, V. Barone M. Cossi, R. Cammi, B. Munnucci, C. Pomelli, C. Adamo, S. Clliford, J. Ochterski, G. A. Petersson, P. Y. Ayala, Q. Cui, K. Morokuma, N. Rega, P. Salvador, J. J. Dannenberg, D. K. Malick, A. D. Rabuck, K. Raghavachari, J. B. Foresman, J. Cioslowski, J. V. Ortiz, A. G. Baboul, B. B. Stefanov, G. Liu, A. Liashenko, P. Pikorz, I. Komaromi, R. Gomperts, R. L. Martin, D. J. Fox, T. Keith, M. A. Al-Laham, C. Y. Peng, A. Nakayakkara, M. Challacombe, P. M. W. Gill, B. Johnson, W. Chen, M. W. Wong, J. L. Andres, C. Gonzalez, M. Challacombe, P. M. W. Gill, B. Johnson, W. Chen, M. W. Wong, J. L. Andres, C. Gonzales, M. Head-Gordon, E. S. Replogle, and J. A. Pople, Gaussian 03, Revision C. 02 ed., (Gaussian, Inc., Pittsburgh, PA 2004).
[67] A. D. Becke, J. Chem. Phys. **98**, 5648 (1993).
[68] R. G. Parr and W. Yang, *Density Functional Theory of Atoms and Molecules* (Oxford University Press, Oxford, 1989).
[69] B. Yang, C. Q. Huang, L. X. Wei, J. Wang, L. S. Sheng, Y. W. Zhang, F. Qi, W. X. Zheng, and W. K. Li, Chem. Phys. Lett. **423**, 321 (2006).
[70] L. X. Wei, B. Yang, R. Yang, C. Q. Huang, J. Wang, X. B. Shan, L. S. Sheng, Y. W. Zhang, F. Qi, C. S. Lam, and W. K. Li, J. Phys. Chem. A **109**, 4231 (2005).
[71] P.J. Linstrom and W.J. Mallard, NIST Chemistry Webbook, National Institute of Standard and Technology, No. 69, Gaithersburg, MD, 2005, http://webbook.nist.gov
[72] P. M. Guyon and J. Berkowitz, J. Chem. Phys. **54**, 1814 (1971).
[73] K. F. Geoghegan and M. A. Kelly, Mass Spectrom. Rev. **24**, 347 (2005).
[74] D. I. Papac and Z. Shahrokh, Pharm. Res. **2**, 131 (2001).
[75] D. B. Kassel, Chem. Rev. **101**, 255 (2001).
[76] B. K. Matuszewski, M. L. Constanzer, and C. M. Chavez-Eng, Anal. Chem. **70**, 882 (1998).
[77] M. Yamashita and J. B. Fenn, J. Phys. Chem. **88**, 4671 (1984).
[78] I. I. Salem, W. A. Saif, Y. Jmeian, and J. I. Al-Tamimi, J. Pharm. Biomed. Anal. **37**, 1073 (2004).
[79] Y. Hsieh, K. Merkle, G. Wang, J. Brisson, and W. A. Korfmacher, Anal. Chem. **75**, 3122 (2003).
[80] I. I. Salem, W. A. Saif, Y. Jmeian, and J. I. A. Tamimi, J. Pharm. Biomed. Anal. **37**, 1073 (2004).
[81] L. M. Zhao, L. G. Hu, Y. Jiang, J. Wang, L. Wang, and J. K. Gu, Chin. J. Anal. Chem. **34**, 1599 (2006).
[82] M. Rafii, R. Elango, G. Courtney-Martin, J. D. House, L. Fisher, and P. B. Pencharz, Anal. Biochem. **371**, 71 (2007).
[83] X. Y. Chen, D. F. Zhong, Y. Han, and Z. Y. Xie, Rapid Commun. Mass Spectrom. **17**, 192 (2003).
[84] H. C. Bi, L. Z. Zhao, G. P. Zhong, S. F. Zhou, B. Li, Y. Deng, X. Chen, and M. Huang, Rapid Commun. Mass Spectrom. **20**, 1153 (2006).
[85] J. M. Lecomte, J. Costentin, A. Vlaiculescu, P. Chaillet, H. Marcais-Collado, C. Llorens-Cortes, M. Leboyer, and J. C. Schwartz, J. Pharmacol. Exp. Ther. **237**, 937 (1986).
[86] Y. Xu, H. C. Huang, F. Liu, S. Gao, and Q. X. Guo, J. Chromatogr. B **852**, 101 (2007).
[87] R. C. Pierce and M. Katz, Environ. Sci. Technol. **10**, 45 (1976).
[88] J. N. Pitts Jr, D. Grosjean, T. M. Mischke, V. F. Simmon, and D. Poole, Toxicol. Lett. **1**, 65 (1977).

Downloaded At: 15:33 21 January 2011

[89] A. Mosi, K. J. Reimer, and G. K. Eigendorf, Talanta **44**, 985 (1997).
[90] S. Patai, *The Chemistry of Quinonoid Compounds* (Wiley, New York, 1974).
[91] X. W. Lou, R. W. Sinkeldam, W. van Houts, Y. Nicolas, P. G. A. Janssen, J. L. J. van Dongen, J. A. J. M. Vekemans, and E. W. Meijer, J. Mass Spectrom. **42**, 293 (2007).
[92] M. Puchalska, M. Orlińska, M. A. Ackacha, K. Poteć-Pawlak, and M. Jarosz, J. Mass Spectrom. **38**, 1252 (2003).
[93] N. Noji, T. Nakamura, N. Kitahata, K. Taguchi, T. Kudo, S. Yoshida, M. Tsujimoto, T. Sugiyama, and T. Asami, J. Agric. Food Chem. **55**, 7258 (2007).
[94] R. Vessecchi, P. G. B. D. Nascimento, J. N. C. Lopes, and N. P. Lopes, J. Mass Spectrom. **41**, 1219 (2006).
[95] R. Geyer, A. D. Peacock, D. C. White, C. Lytle, and G. J . Van-Berkel, J. Mass Spectrom. **39**, 922 (2004).
[96] M. J. Dale, A. C. Jones, P. R. R. Langridge-Smith, K. F. Costello, and P. G. Cummins, Anal. Chem. **65**, 793 (1993).
[97] J. H. Beynon, G. R. Lester, and A. E. Williams, J. Phys. Chem. **63**, 1861 (1959).
[98] C. J. Proctor, B. Kralj, E. A. Larka, C. J. Porter, A. Maquestiau, and J. H. Beynon, Org. Mass Spectrom. **16**, 312 (1981).
[99] W. G. Stensen and E. Jensen, J. Mass Spectrom. **30**, 1126 (1995).
[100] J. H. Bowie, D. W. Cameron, and D. H. Williams, J. Am. Chem. Soc. **87**, 5094 (1965).
[101] J. H. Beynon and A. E. Williams, Appl. Spectrosc. **14**, 156 (1960).
[102] M. L. Ferreiro and J. Rodríguez-Otero, J. Mol. Struct. (Theochem) **542**, 63 (2001).
[103] G. Nelson, J. Chandrashekar, M. A. Han, L. Feng, G. Zhao, N. J. P. Ryba, C. S. Zuker, Nature **416**, 199 (2002).
[104] A. Brack, *The Molecular Origins of Life* (Cambridge University Press, Cambridge, UK, 1998).
[105] D. Shemesh and R. B. Gerber, J. Chem. Phys. **122**, 241104 (2005).
[106] V. Vorsa, T. Kono, K. F. Willey, and N. Winograd, J. Phys. Chem. B **103**, 7889 (1999).
[107] A. F. Lago, L. H. Coutinho, R. R. T. Marinho, A. Naves de Brito, and G. G. B . de Souza, Chem. Phys. **307**, 9 (2004).
[108] A. G. Császár, J. Phys. Chem. **100**, 3541 (1996).
[109] L. Claes, J. P. François, and M. S. Deleuze, J. Am. Chem. Soc. **125**, 7129 (2003).
[110] S. Knippenberg, B. Hajgató, J. P. François, and M. S. Deleuze, J. Phys. Chem. A **111**, 10834 (2007).
[111] P. Ehrenfreund, D. P. Glavin, O. Botta, G. Cooper, and J. L. Bada, Proc. Natl. Acad. Sci. USA **98**, 2138 (2001).
[112] S. X. Tian, J. Phys. Chem. A. **110**, 3961 (2006).
[113] M. E. Sanz, A. Lesarri, M. I. Peña, V. Vaquero, V. Cortijo, J. C. López, and J. L. Alonso, J. Am. Chem. Soc. **128**, 3812 (2006).
[114] S. J. McGlone and P. D. Godfrey, J. Am. Chem. Soc. **117**, 1043 (1995).
[115] M. A. Wagner and M. S. Jorns, Biochem. **39**, 8825 (2000).
[116] H. J. Guo, L. D. Zhang, L. L. Deng, L. Y. Jia, Y. Pan, and F. Qi, J. Phys. Chem. A. **114**, 3411 (2010).
[117] J. M. Dietschy and S. D. Turley, J. Lipid. Res. **45**, 1375 (2004).
[118] C. P. Cannon, Clin. Cornerstone **8**, 11 (2007).
[119] W. J. Griffiths, Mass Spectrom. Rev. **22**, 81 (2003).
[120] Y. Q. Wang, M. Hornshaw, G. Alvelius, K. Bodin, S. Y. Liu, J. Sjövall, and W. J. Griffiths, Anal. Chem. **78**, 164 (2006).
[121] G. J. Van-Berkel, J. M. E. Quirke, R. A. Tigani, A. S. Dilley, and T. R. Covey, Anal. Chem. **70**, 1544 (1998).
[122] G. Singh, A. Gutierrez, K. Xu, and I. A. Blair, Anal. Chem. **72**, 3007 (2000).
[123] M. Careri, D. Ferretti, P. Manini, and M. Musci, J. Chromatogr. A **794**, 253 (1998).

Downloaded At: 15:33 21 January 2011

[124] S. Acevedo, L. B. Gutierrez, G. Negrin, J. C. Pereira, B. Mendez, F. Delolme, G. Dessalces, and D. Broseta, Energy Fuels **19**, 1548 (2005).
[125] R. Tanaka, S. Sato, T. Takanohashi, J. E. Hunt, and R. E. Winans, Energy Fuels **18**, 1405 (2004).
[126] E. Al-Muhareb, T. J. Morgan, A. A. Herod, and R. Kandiyoti, Pet. Sci. Technol. **25**, 81 (2007).
[127] A. R. Hortal, B. Martinez-Haya, M. D. Lobato, J. M. Pedrosa, and S. Lago, J. Mass Spectrom. **41**, 960 (2006).
[128] B. Martinez-Haya, A. R. Hortal, P. Hurtado, M. D. Lobato, and J. M. Pedrosa, J. Mass Spectrom. **42**, 701 (2007).
[129] M. Millan, M. Behrouzi, F. Karaca, T. J. Morgan, A. A. Herod, and R. Kandiyoti, Catal. Today **109**, 154 (2005).

Downloaded At: 15:33 21 January 2011